Delft University of Technology
Faculty of Aerospace Engineering
Delft

Prins Maurits Laboratory
Organization for Applied
Scientific Research TNO
Rijswijk

Report LR -514
Report PML 1987 - C18
SFCC PUBLICATION NO. 42

COMBUSTION OF PMMA, PE AND PS IN A RAMJET

C.W.M. van der Geld
P.A.O.G. Korting
T. Wijchers

Delft/Rijswijk, The Netherlands

April 1987

Delft University of Technology
Faculty of Aerospace Engineering
Delft

Prins Maurits Laboratory
Organization for Applied
Scientific Research TNO
Rijswijk

Report LR -514
Report PML 1987 - C18
SFCC PUBLICATION NO. 42

COMBUSTION OF PMMA, PE AND PS IN A RAMJET

C.W.M. van der Geld
P.A.O.G. Korting
T. Wijchers

Delft/Rijswijk, The Netherlands

April 1987

TABLE OF CONTENTS

NOMENCLATURE

Standard conditions:

L	= 300 mm
d_{po}	= 40 mm
h/d_{po}	= 0,3125
m_a	= 150 g/s
P_c	~ 0,9 MPa
T_{in}	= 286 ± 7 K

aft mixing chamber length 170 mm

List of symbols

c^*	characteristic velocity (eq. 3.3.2 and 3.3.3)
D	inner grain diameter (m)
d_{po}	initial port diameter (m)
G	average total mass flux (kg/m^2s)
h	stepheight (m)
$h_{v_{eff}}$	effective heat of gasification (J/kg)
L	grain length (m)
m_{air}	air mass flow rate (kg/s)
m_f	fuel mass flow rate (kg/s) (eq. 3.3.4)
O/F	ratio of (oxygen enriched) air and fuel, mass based
p	pressure
$p_c = P_c$	mean combustion pressure in aft mixing chamber
q_c	convective heat transfer
q_r	radiative heat transfer
q_w	heat transfer to fuel surface
r	regression rate
T	temperature
T_f	flame temperature
T_{inlet}	air inlet temperature
T_r	radiation temperature
T_{wall}	wall temperature
γ	ratio of specific heats, C_p/C_v
Γ	Vandenkerkhove function (eq. 3.3.5)

ε_g	emission coefficient of the gasmixture radially observed
ε_w	wall absorption coefficient
η	combustion efficiency (eq. 3.3.1)
ρ	mass density (kg/m^3)
ρ_F	fuel mass density (kg/m^3)
ϕ	mixture ratio (eq. 3.3.6)
σ	Stephan Boltzman constant

Acronyms

PE	polyethylene
PMMA	polymethylmethacrylate
PS	polystyrene
SCMC	sonic control and measuring choke
SFCC	solid fuel combustion chamber
SFRJ	solid fuel ramjet

ABSTRACT

The combustion behaviour of polymethylmethacrylate (PMMA), polyethylene (PE) and polystyrene (PS) was investigated in a connected pipe test facility. Instantaneous and local regression rates were determined. Spectroscopy was applied, showing inter alia the occurrence of OH, C_2 and CH and temperatures between 1300 and 3000 K during combustion.
Main issues of the present investigation are the establishing and understanding of the most important phenomena that control or emanate from the combustion of a cylindrical solid fuel with a rearward facing step. Main utilization is for solid fuel ramjets, safe burning of toxic waste and hot gas generators. During the investigation attention was focussed on

- regression rate
- efficiency
- temperatures
- soot production.

At pressures between ± 0,6 and ± 1,1 MPa, radiative heat transfer from soot causes an increase of regression rate for PMMA and PE. At pressures below 0,5 MPa hardly any soot was observed during combustion of PMMA and PE. PS was already sooting.

The combustion efficiency varied from 70 to 90 %. Efficiency depended on oxygen content, fuel grain length and composition of the fuel.

The large vortex structure downstream of the sudden expansion at the inlet was shed at a regular rate. This phenomenon was found to be essentially two-dimensional and to correspond to temperature fluctuations of 200 K in the downstream end of the chamber and of 600 K in the upstream end.

1 INTRODUCTION

A joint research programme is being carried out by the Faculty of Aerospace Engineering of Delft University of Technology and the Prins Maurits Laboratory TNO. The combustion behaviour is investigated of various solid fuels in a connected pipe test facility. The programme encompasses both theoretical (ref. 8) and experimental work and is aimed at a better understanding of the flow and combustion processes, and their mutual interaction, in solid fuel combustion chambers.

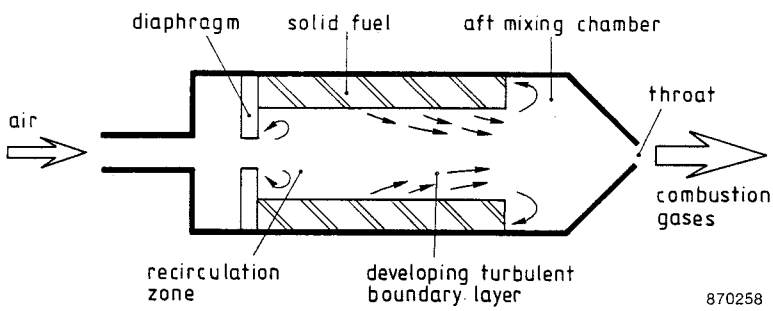

Figure 1.1.
Schematic of a solid fuel ramjet combustion chamber.

Figure 1.1 is a schematic of a SFRJ combustion chamber. Air enters through lines as indicated. Directly downstream of the diaphragm a recirculation zone is established. The fuel pyrolyses and fuel gases mix and react with the oxidizer. Combustion products with air pass through an aft mixing chamber and are exhausted through a nozzle.

Experiments were performed with the following fuels:

- polymethylmethacrylate (PMMA);
- polystyrene (PS);
- polyethylene (PE);

by burning with

- ambient air;
- oxygen enriched air;
- air at elevated temperatures.

Emphasis was laid on the effects of pressure, mass flow rate and configurational parameters on regression rate and combustion efficiency. The results were interpreted and related to the relative importance of the various heat transfer, flow and combustion mechanisms prevailing in a solid fuel combustion chamber. The combustion efficiency was examined as a measure of the deviation from complete combustion (equilibrium flow). The combustion behaviour of the three fuels were compared with each other.

2 TEST FACILITY AND DATA ACQUISITION

2.1 TEST RIG

Figure 2.1 shows a schematic of the main parts of the test facility. Not shown are feeding lines with especially developed flow meters, Sonic Control and Measuring Chokes (SCMC's). The SCMC's are computer controlled, guarantee constant total mass flow rates (± 3%) and allow for accurate flow rate measurements. A vitiator can burn methane with oxygen enriched air, and produces air at elevated and precisely controlled temperatures. The oxygen content of the exhaust gases can be varied, but typically corresponds to that of ambient air.

A shuttle valve was opened towards the solid fuel combustion chamber (SFCC) as soon as the vitiator was functioning stably with proper exhaust gases.

In the SFCC hollow cylindrical fuel grains were mounted, and flame stabilization was achieved by a rearward facing step. Chamber pressure was varied by adjusting the nozzle throat diameter. Grain length's and the length of the aft mixing chamber could be varied.

The sequence of events during each test run was controlled by computer. In case of anomalies or safety hazards, a test run was automatically interrupted.

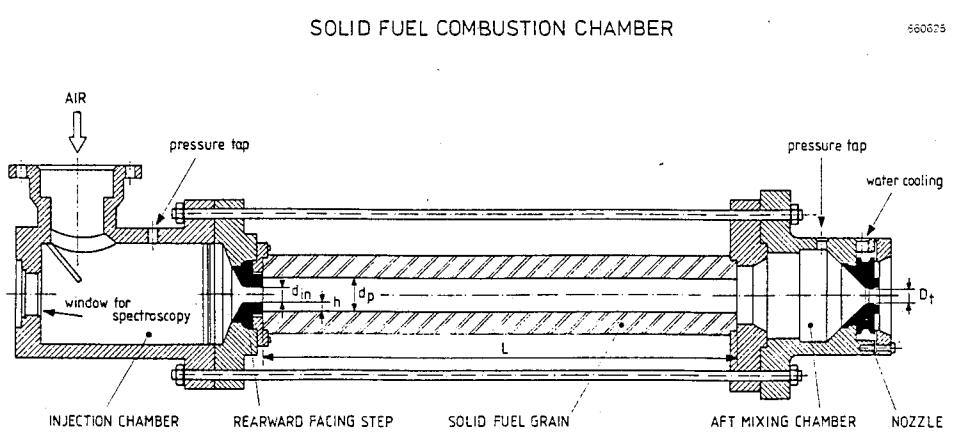

Figure 2.1a
Schematic of the solid fuel combustion chamber.

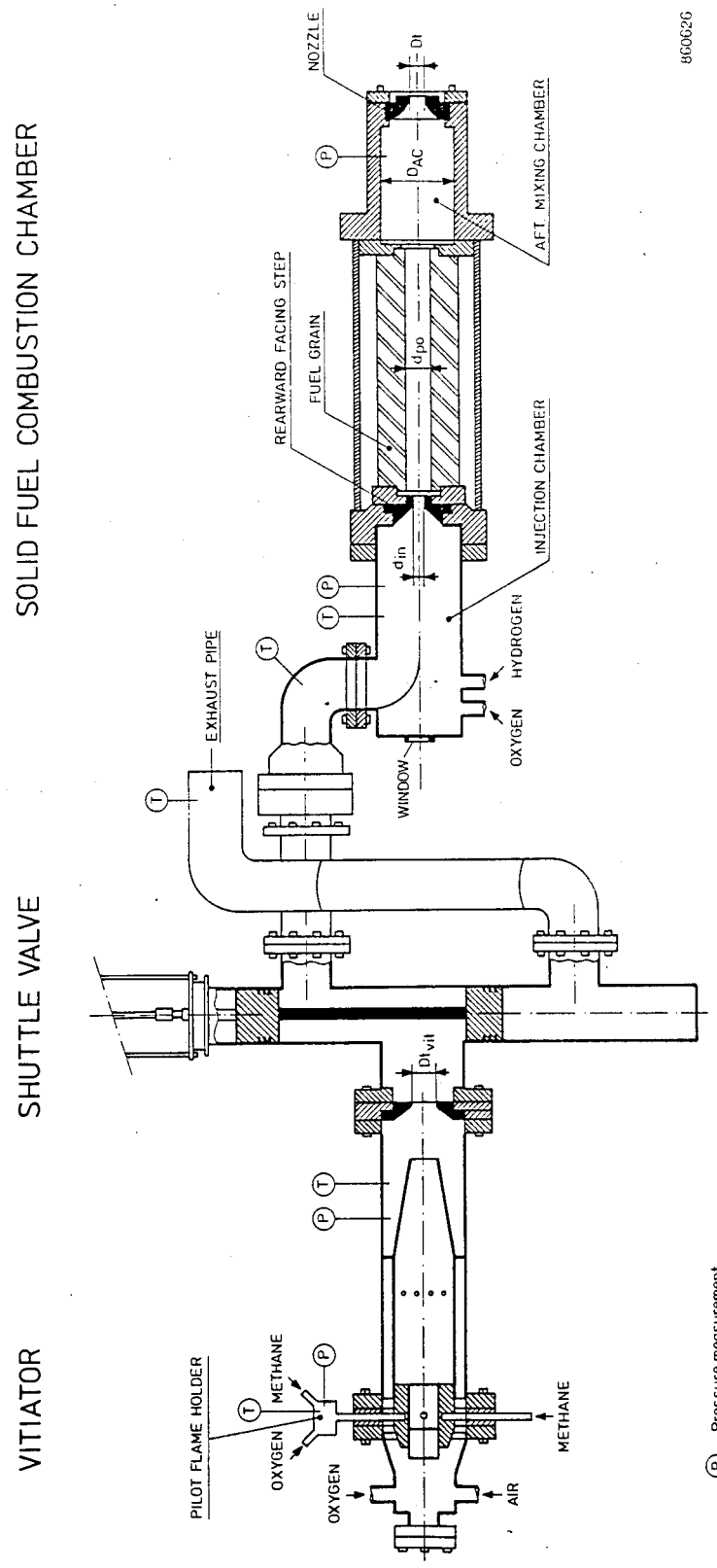

Figure 2.1b

Schematic of the test facility used.

2.2 INSTRUMENTATION

2.2.1 Data registration

During each test run the following parameters were recorded on an ultraviolet recorder and on digital and analogue tape recorders:

- temperatures (see figure 2.1)
- pressures (see figure 2.1)
- mass flow rates of air, oxygen and methane (SCMC's, see section 2.1).

After burning, the weight loss of the grain was measured as well as the grain inner surface profile. These data were filed together with the digitized output from tape recorders. Resulting files were labeled in the same manner as the floppy disk files that contain corresponding spectroscopic data (see section 2.2.2.).

2.2.2 Optical intrumentation

2.2.2.1 Video- and cinefilms. Video was used to monitor the combustion process and to register accidents and special events. During selected test runs, high speed cine cameras were operated at a speed of 10 kcps.

2.2.2.2 Spectroscopy. Spectroscopic equipment (see figure 2.2) was used to measure

- the occurrence of species during combustion
- chordal beam averaged temperatures (mirror M2 above the SFCC and S')
- axis averaged temperatures (mirrors M1 and M2).

As depicted in Fig. 2.2, light passes through lens L1 and, via mirrors M3 and M4, through a hole in the wall of the testroom. Subsequently the light is brought by lens L2 on the entrance slit S of a 1 m grating spectrograph (Jobin Yvon THR 1000 S, 600 l/mm and 2400 l/mm). For spectral calibration, the radiation of spectral lamp Li2 can be brought to S via L4 and by inserting M5.

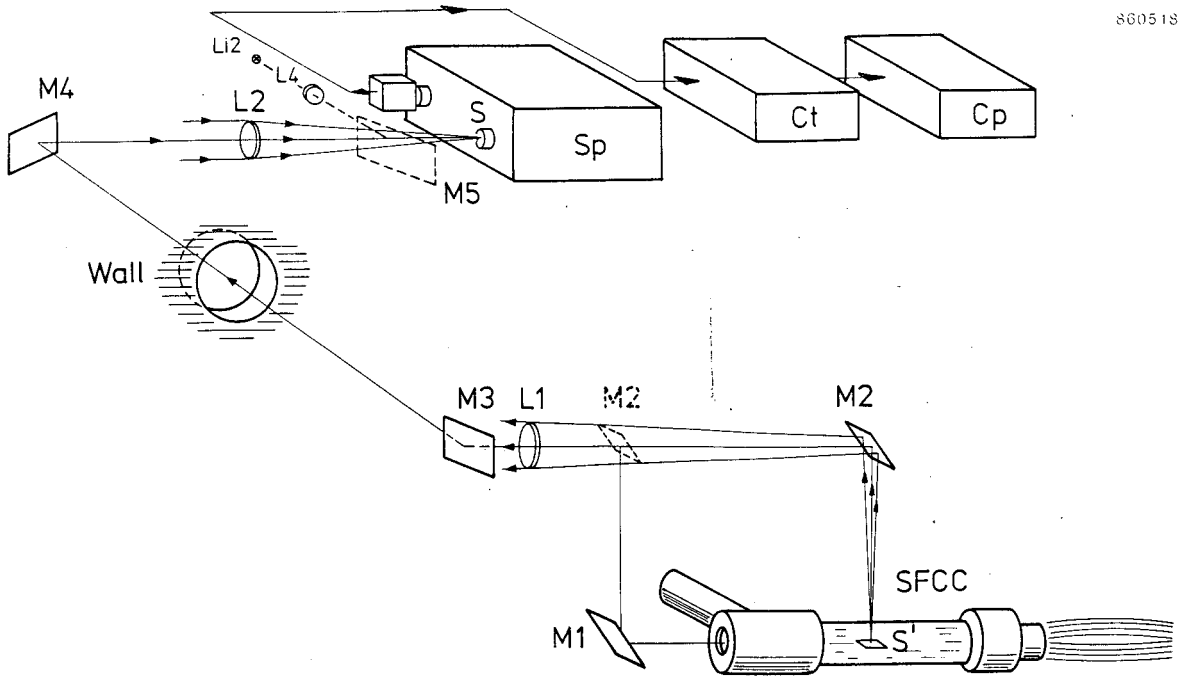

Figure 2.2
Schematic of optical train, spectrograph and processing equipment.

The focus of L2 is permanently fixed on S, while the other optical components are adjusted in such a way that the image S' of S is brought at the proper location in the combustion chamber at maximum efficiency. A multichannel detector D with an intensifier (SI IRJ 1024, 1024 channels on 25 mm), is read out after each exposure by controller Ct. This controller can store up to 32 spectra which are successively recorded by the detector. A personal computer Cp processes the recorded spectra. The efficiency of the optical train between S and S' (distance about 10 m) is about 30%. The spectrograph, L2 and M4 are fixed on a heavy granite table in a separate room, while the other components of the optical train are mounted on a single optical bench. More details have been given by Wijchers (ref. 1).

2.2.2.3 Pyrometry. The temperature of the flame in the SFCC is determined from the radiation intensities of soot at two different wavelengths. Hence the so called colour-temperature is obtained.

The colour-temperature of a radiator is defined as the temperature of a black body that emits radiation with the same spectral intensity ratio at specific wavelengths as the actual radiator does.
Soot particles can be regarded as black radiators, considering their structure and colour at room temperatures. Furthermore, it is assumed that the difference between gas temperature and soot temperature is negligible.

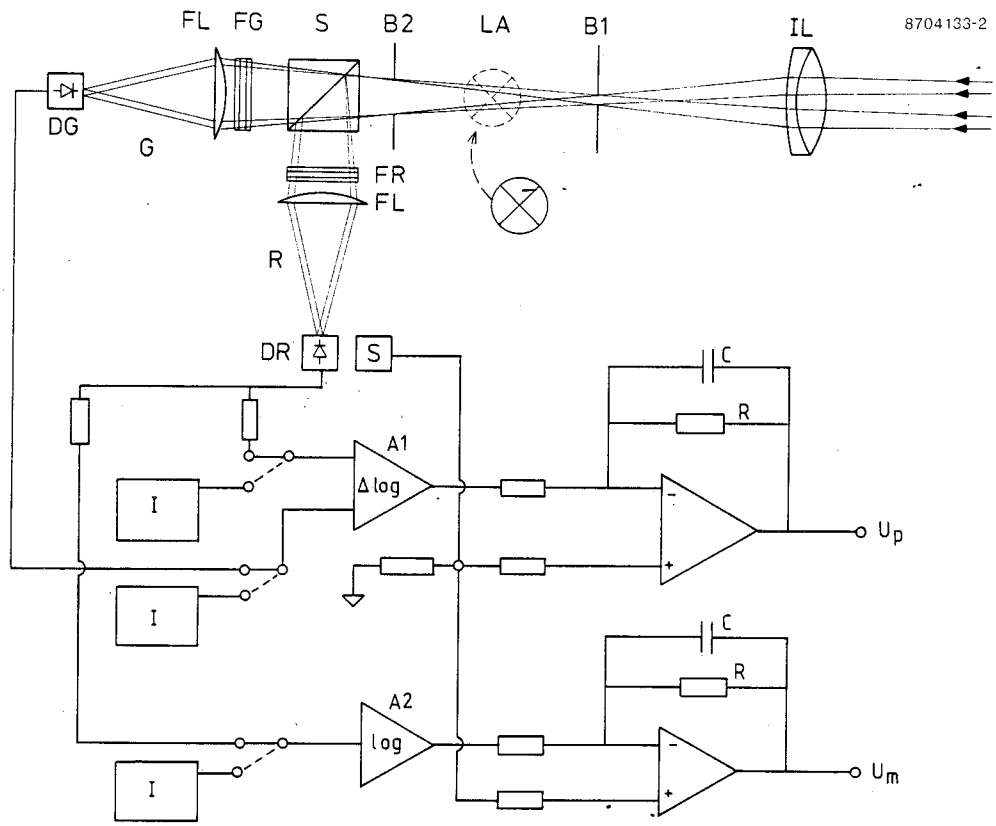

Figure 2.3
Schematic of the two-colour pyrometer.

Figure 2.3 is a schematic of the two-colour pyrometer, built in our laboratory. Radiation through lens IL is split into two almost equal parts by beamsplitter S. Interference filters FR and FG are transparent only at central wavelengths 830 nm and 577 nm respectively with a bandwith of 10 nm. They guarantee that no atomic and molecular radiation from the flame can be detected by the silicon detectors DR and DG.
The images of the opening of B1, together with the sferical aberration formed by the field lenses FL, are well within the sensitive areas of the detectors.

The dimensions of beam splitter S, the filters FR, FG, and the field lenses FL are such that any ray, passing B1 and B2 (and for which a filter is transparent), will reach the detector behind that filter. The area of detection is the image at the radiator of the opening of B1 formed by IL. The area of detection as well as the solid angle of detection from that area are completely determined by B1 and B2 and hence equal for both detectors.
The area of detection appears as a lightspot if lamp LA is swung in. In order to direct the pyrometer, it is brought into such a position that the lightspot covers that part of the SFCC, of which the temperature must be determined.
The distance between IL and B1 can be varied in 5 steps causing the diameter of the area of detection to vary from 4 mm to 80 mm at distances from 0,2 to 2 m respectively.

The current from detector DR is divided by two high ohmic resistors to amplifiers A1 and A2, while detector DG, providing the smallest current of the two, is directly connected to A1. The output of the commercially available amplifier A1 is the logarithm of the ratio of the currents at both inputs, while the signal from A2 is proportional to the logarithm of its input current. The signals from A1 and A2 are fed to inverting amplifiers, to form the pyrometer output U_p and monitor output U_m respectively. The bandwidths are limited by RC-filters.

The time constant of the log-amplifiers increases to 0.01 s for to 1nA decreasing input currents. For that reason, the time constant of the RC filters in the differential amplifier both are set to 0.01 s.
The output of a temperature sensor, located close to the red detecting detector, was also fed into the differential amplifiers for the pyrometer signal in order to compensate for the temperature dependance of the spectral sensitivity of the detectors and the temperature dependance of the logarithmic amplifiers.
The pyrometer was calibrated against a (colour) temperature-calibrated tungsten ribbon lamp. The output volgate therefore is a well known function of the colour temperature.
The accuracy obtained is 10 K - 20 K.
The reliability of the current ratio measurement by the amplifiers can be examined by switching both inputs to the current sources I. These two sources together consist of only one voltage source with several resistors to be

switched at will. The stability of the current ratio depends only on the stability of the value ratio of high-quality resistors used.

3 MEASUREMENT RESULT AND DISCUSSION

3.1 GENERAL COMBUSTION BEHAVIOUR

3.1.1 Visual observations

Both video and high speed cine recordings clearly showed that light emission during combustion of PMMA starts in the recirculation zone and proceeds downstream until the entire grain exhibits the combustion process. Visual observations of PE and PS showed the same. Figure 3.1.1 is a typical pressure history and idicates that about 15 s are required indeed to obtain a fully developed flame.

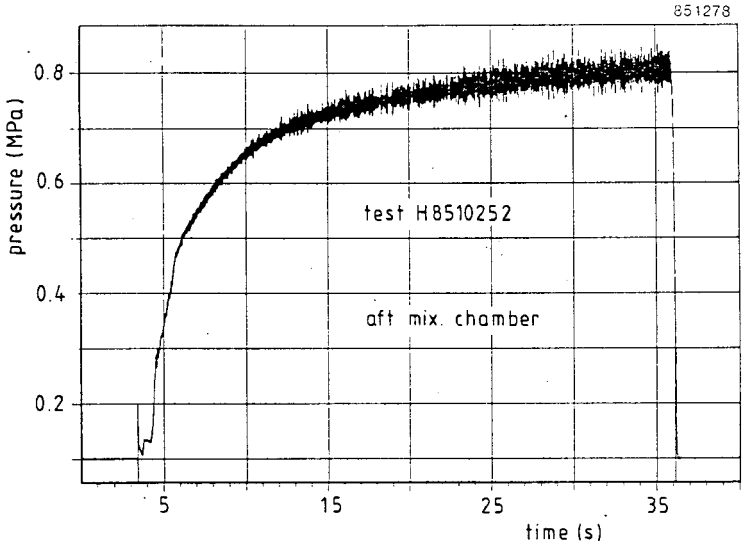

Figure 3.1.1
Specimen of chamber pressure history.

The initial pressure peak is due to ignition.
At pressures below 0,5 MPa, emitted radiation for PMMA and PE was blue, indicating hardly any soot formation. At higher pressures the flame became yellow because of soot.

High speed cine-recordings clearly revealed the shedding of the vortices that fill up the recirculation zone directly downstream of the sudden expansion (see figure 3.1.2).

The shedding frequency was dependent mainly on inlet geometry, but typical values were in the range 70-100 Hz. The use of elongated mirror plates on both sides of the fuel grain revealed that the vortex structure was essentially two dimensional.
Light emission measurements not only showed a gradual increase of total light emission during burning, but also strong oscillations at frequencies in the range 70-100 Hz (see figure 3.1.3).

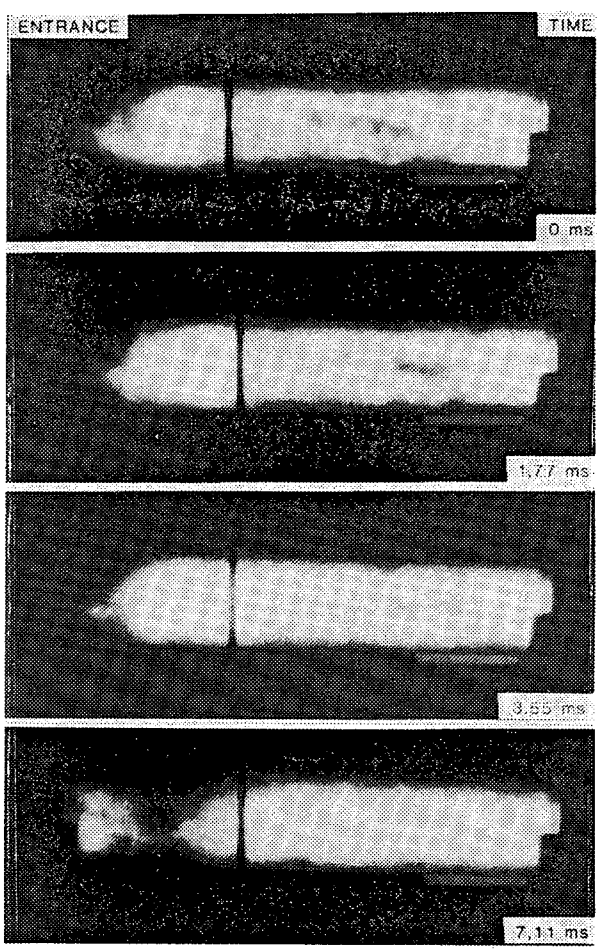

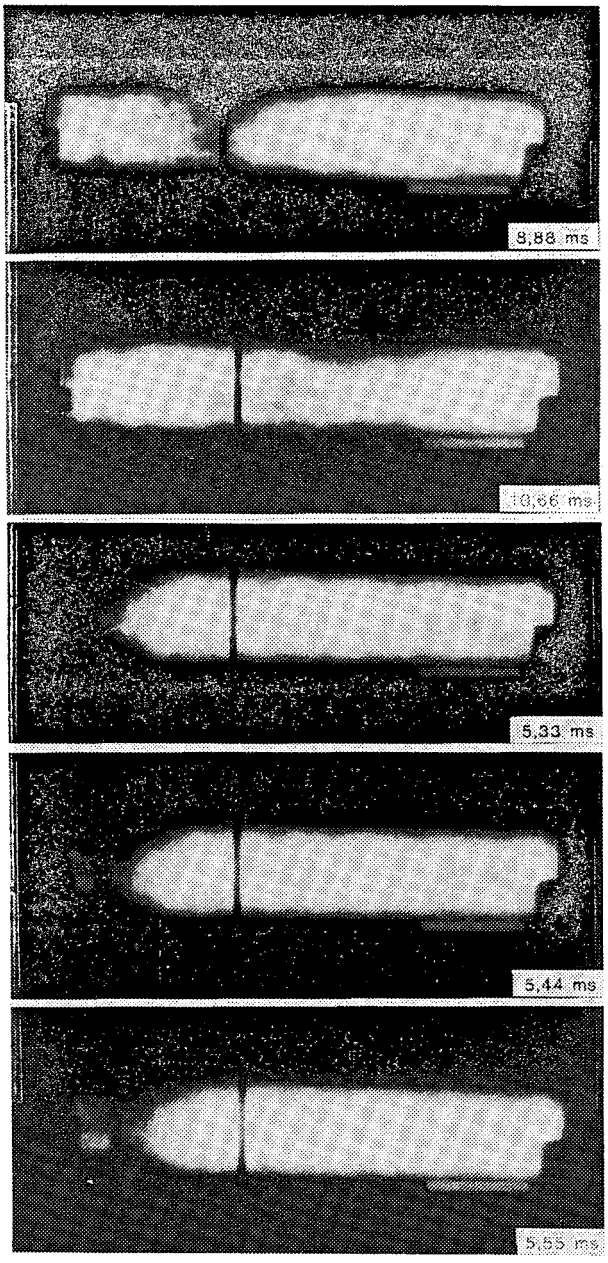

Figure 3.1.2

Shedding of the coherent structure from the recirculation zone.

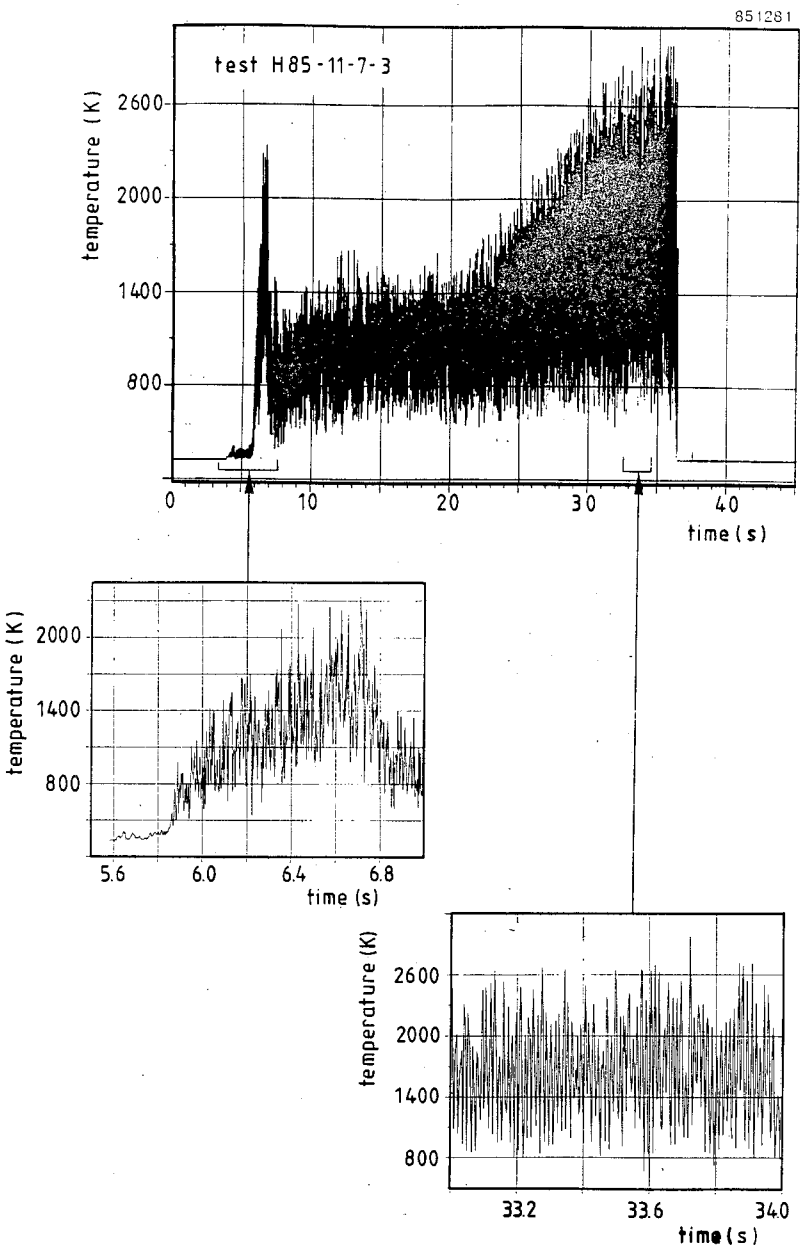

Figure 3.1.3

Radiative temperature history measured by a radiation detector PMMA/ambient air; P_c = 0,9 MPa.

The same oscillatory behaviour was also detected from pressure recordings. If the combustor was forced to operate in a "chugging" mode corresponding to standing acoustical waves with frequencies of ca. 1000 Hz, the amplitude of

pressure oscillations at ca. 80 Hz. due to the vortex shedding phenomenon was even strongly enhanced (see fig. 3.1.4.).

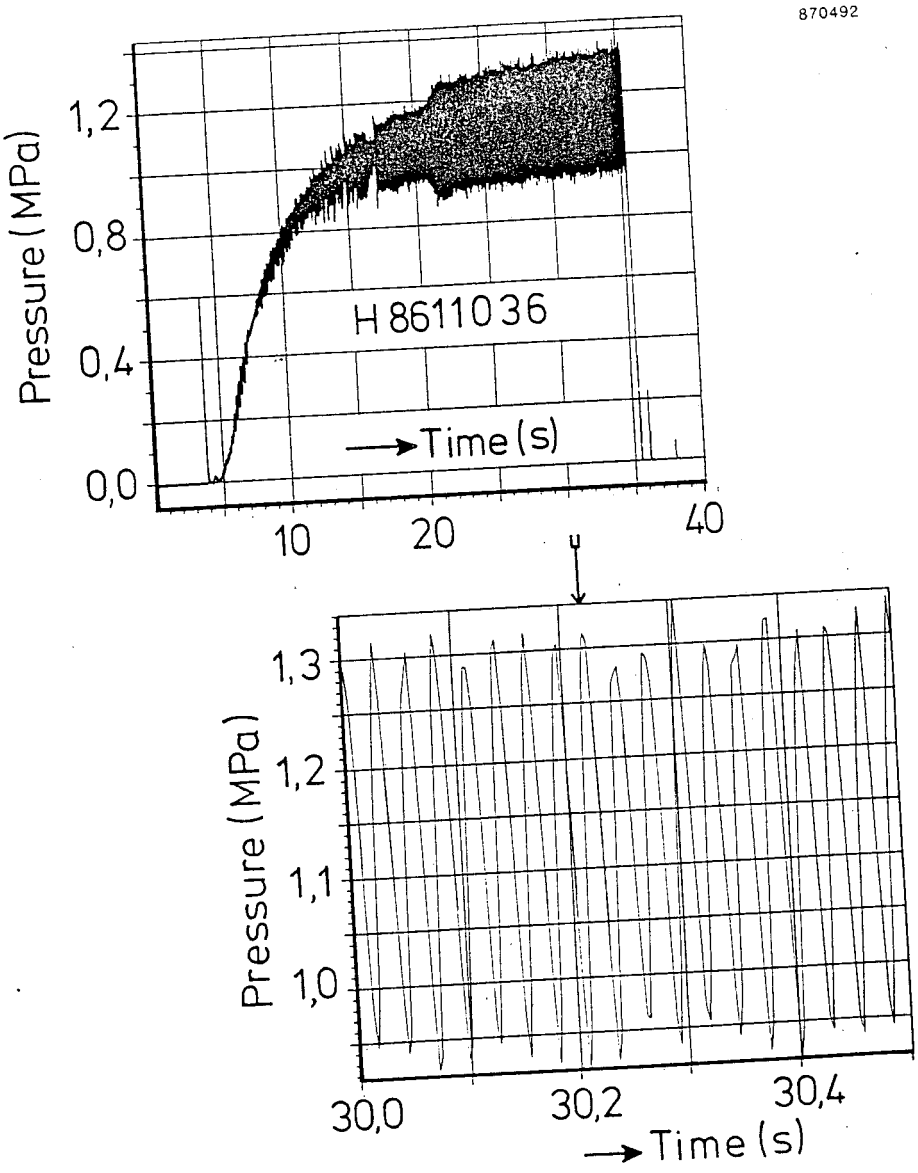

Figure 3.1.4
Specimen of the pressure history during "chugging" combustion.

The vortex shedding frequency was not affected by the occurrence of this chugging. The shedding frequency was substantially reduced to about 40 Hz only after the introduction of an elongated inlet section. This is discussed more fully by Van der Geld (1987, ref. 2).

3.1.2 Inner grain profiles

The internal surface profile of fuel grains was measured after each test run. For the fuels investigated, PMMA, PE and PS, the surface outside the recirculation zone remained almost parallel to the center line (see figure 3.1.5.).

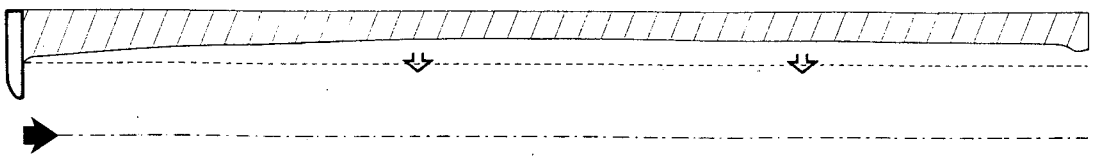

Figure 3.1.5
Inner surface profile after combustion.

The region of homogeneous burning begins at a distance of about 9 stepheights from the entrance. This reattachment point is a kind of stagnation point where boundary layers begin to develop, and where convective heat transfer and hence regression rate are usually higher than at places where flow is fully developed. In the recirculation zone, regression is less because of lower velocities. Dowstream of the reattachment point, however, the flow is accelerated by the injected fuel, and convection is enhanced by the increasing velocity. From figure 3.1.5. and other measurements, the latter effect is seen to compensate more or less for the effect of the growing boundary layer, that hampers more or less convective heat transfer.

X-ray fotography revealed the width, ~ 5 µm, of cracks that were observed at the grain inner surface (see figure 3.1.6).

It also showed that these cracks are rather deep, deeper than 5 µm, straight and rather long. The occurrance of these cracks is attributed to the relatively high pressure prevailing in the grain. They could be observed only after removal of the "cold" soot layer that is deposited after stopping the combustion process by closing the valves in the feeding lines. The cracks obviously enlarge the effective, pyrolizing surface area of the grain.

Figure 3.1.6

X-ray photograph of grain inner surface.

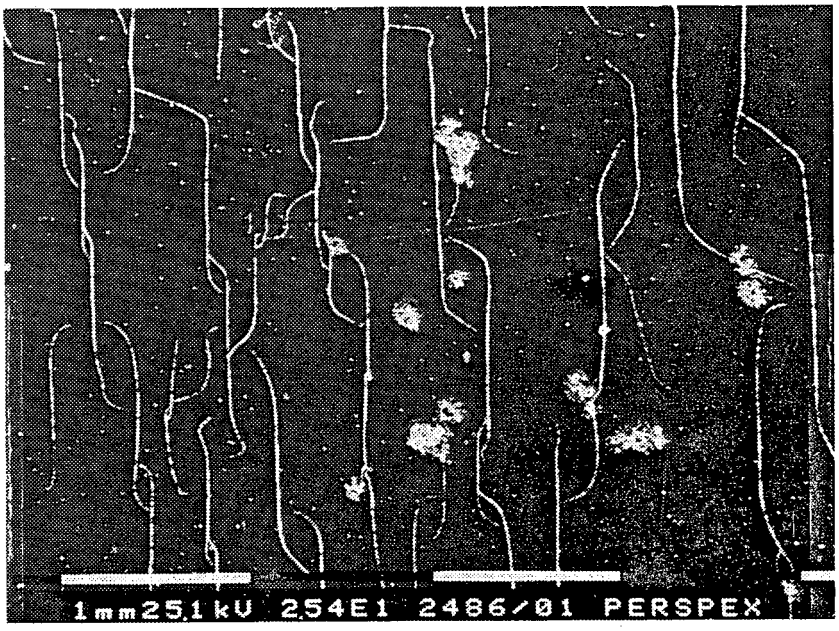

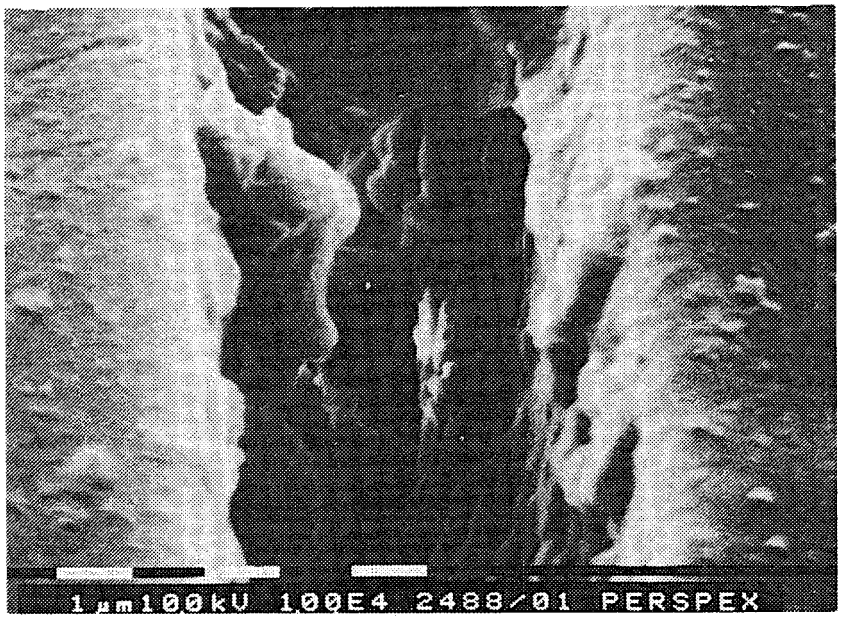

3.2 REGRESSION RATE

The mean regression rate was deduced from

- weight loss of the fuel;
- grain inner profile measurements.

The influence of various flow and configuration parameters on the mean regression rate is discussed in this chapter.

Unless indicated otherwise, experimental results refer to our standard conditions:

- fuel grain length, L : 0,3 m
- initial step height, h_o : 12,5 mm
- initial inner bore diameter, d_{po} : 40 mm
- air mass flow rate, m_a : 150 g/s
- chamber pressure : $\pm$ 0,9 MPa

- aft mixing chamber length: 0,17 m
- air inlet temperature : 286 $\pm$ 8 K

Each of these parameters was varied keeping the others constant. The only combined effect investigated is that of pressure and mass flow rate.

3.2.1 Dependency on fuel composition

In figure 3.2.1 regression rates are compared to PE and PS for various mass fluxes at a pressure level of around 1 MPa.

The results for PE were correlated by

$$(3.2.1) \quad r = 3{,}45.10^{-4}\ m_a^{\,0{,}3105} \qquad (0{,}8 < P_c\ (\mathrm{MPa}) < 1{,}1)$$

with r in m/s and m_a in kg/s. This correlation can also be written as

$$r = 4{,}53.10^{-5}\ \bar{G}^{\,0{,}3123}$$

with r in m/s and $\bar{G}$ in kg/m^2s.

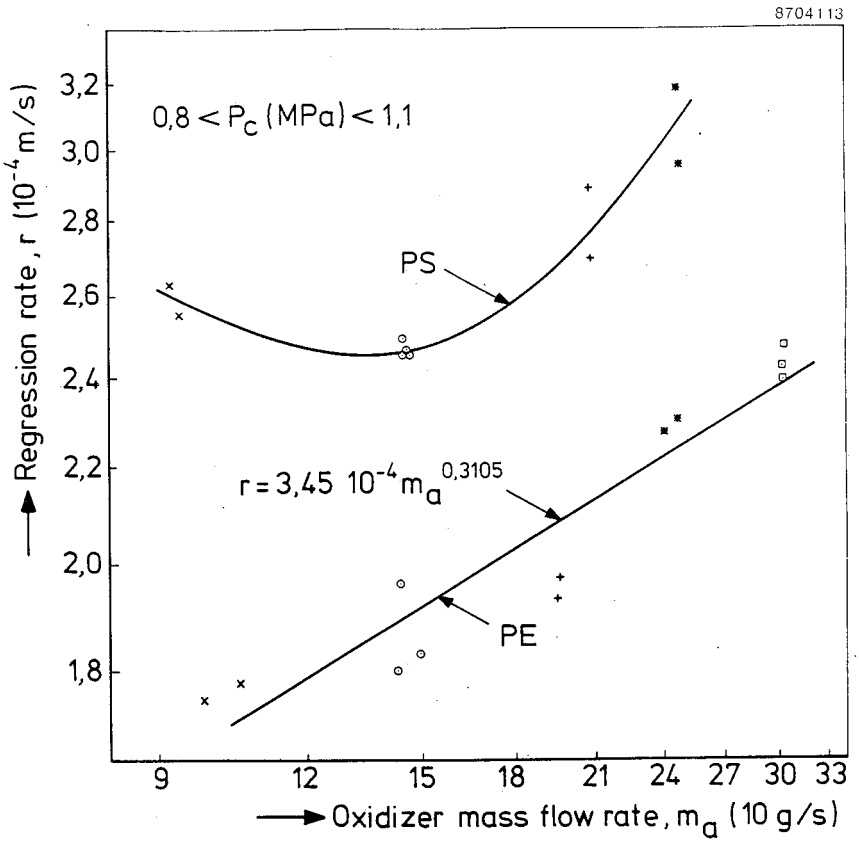

Figure 3.2.1

Effect of mass flux on the regression rate of PE and PS at pressures around 0,9 MPa.

Figure 3.2.1 shows that the regression rate of PS is about 40% larger than that of PE and follows a different trend. In section 3.2.3, the regression rate of PMMA will be seen to be only slightly less than that of PE, and to have the same dependency on mass flow rate, m_a.

However, table 3.2.1 shows that because of differences in the heat of combustion, the heat release of PE combustion gases is substantially higher than that of PMMA gases. This observation may be of particular interest for the utilization of solid fuel combustion chambers. Appendix 1 lists also other physical and chemical properties of all three fuels.

Table 3.2.1: Calculation of typical heat fluxes

	PMMA	PE	PS	unit
regression rate (m_a = 150 g/s; P_c = 1,1 MPa)	0,191	0,220	0,270	mm/s
heat of combustion of gas phase	26,2	46,5	41,5	MJ/kg
mass density	1180	940	1050	kg/m^3
heat fluxes	5,9	9,6	11,8	MW/m^2

At a pressure level of about 0,4 MPa the regression rate of PE was found to be more strongly dependent on mass flow rate (see figure 3.2.2*)). This is also obvious from the exponent in the correlation

$$(3.2.2) \quad r = 5{,}05.10^{-4}\ m_a^{0{,}6310} \qquad (0{,}4 < P_c(\text{MPa}) < 0{,}5)$$

with r in m/s and m_a in kg/s. This correlation can also be written as

$$r = 6{,}09.10^{-6}\ \bar{G}^{0{,}6938}$$

with r in m/s and $\bar{G}$ in kg/m^2s.

No measurements of PS at this pressure level were performed. Again the regression rate of PMMA at this pressure level will be seen (section 3.2.3) to show the same behaviour as that of PE. Figure 3.2.3 shows the effect of chamber pressure on the regression rate of PE and PS at standard conditions. Again the results for PMMA will be seen (section 3.2.3) to almost coincide with those of PE.

*) In this figure and following ones, different symbols for experimental data indicate different experimental conditions (e.g. pressure).

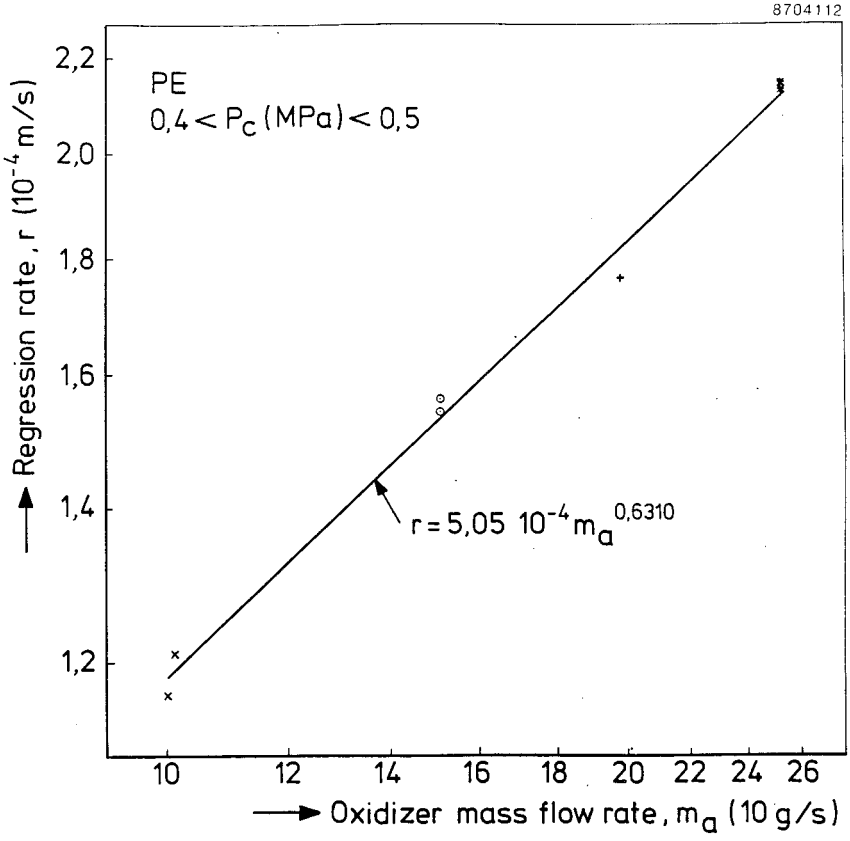

Figure 3.2.2
Effect of mass flux on the regression rate of PE at low chamber pressures.

The regression rate of PS is almost independent of the chamber pressure, whereas the regression rate of PE strongly increases with increasing pressure. The trend for PE and PMMA will be elucidated in section 3.2.2. The nearby plateau burning of PS is often favourable in applications, e.g. ramjets and launch missiles. However, the large soot production of PS (see section 3.1) has then to be prevented, for example by increasing the oxygen content in the oxidizer. The latter will be discussed in sections 3.2.4 and 3.3.3. The combined effects of increasing oxygen content and chamber pressure was not yet investigated.

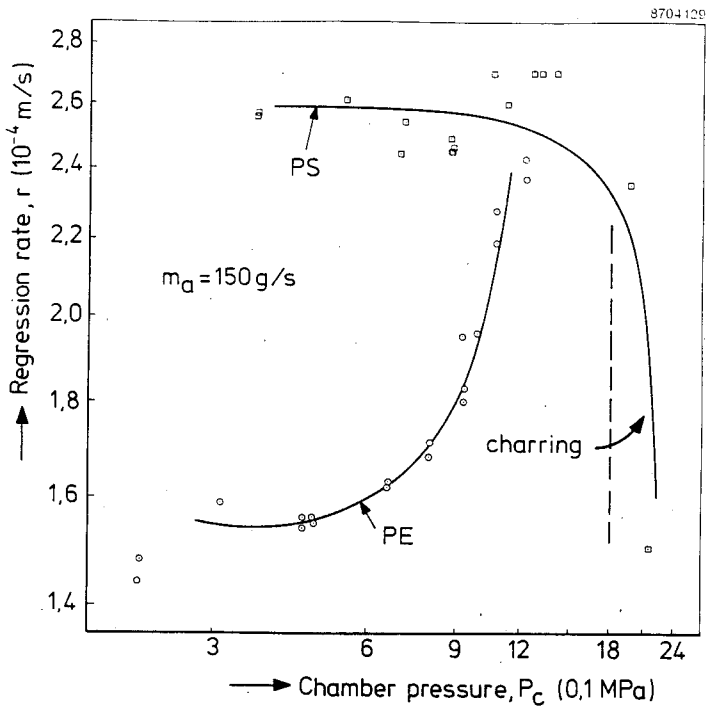

Figure 3.2.3

Effect of pressure on the regression rate of PE and PS; m_a = 150 g/s.

3.2.2 The dependency on chamber pressure for PMMA

Figure 3.2.4 shows the effect of chamber pressure on the regression rate of PMMA. The trent is the same as for PE (see section 3.2.1).

Essentially three different pressure regions are noticed:

(A) P_c < 0,6 MPa

Hardly any pressure sensitivity, although scatter in the results is relatively high.

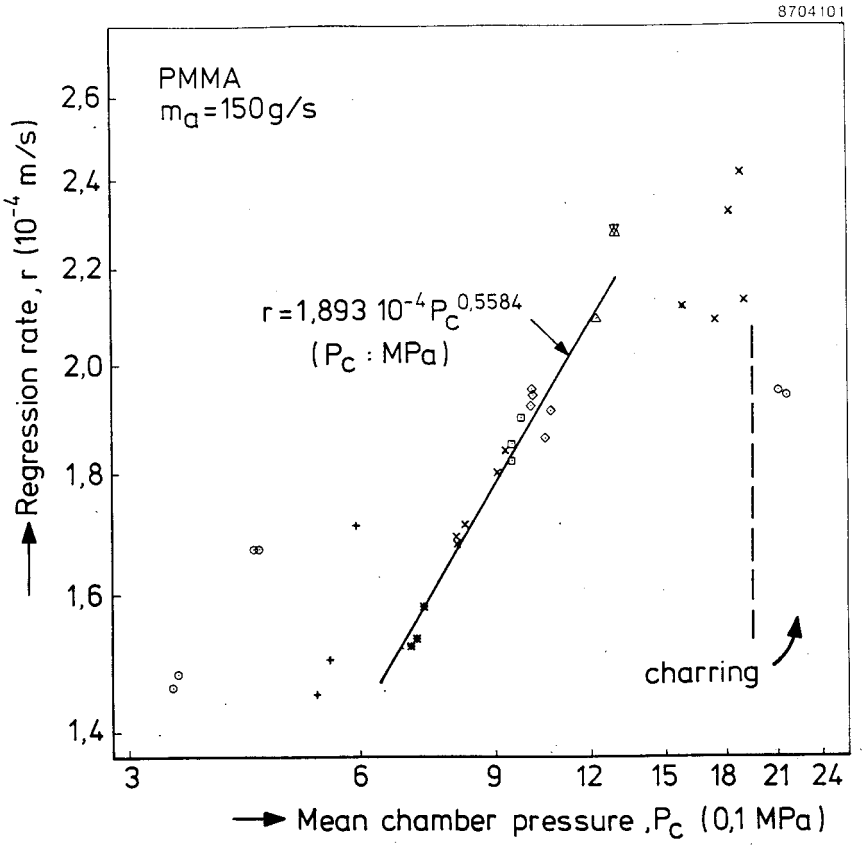

Figure 3.2.4

Effect of chamber pressure on the regression rate of PMMA.

(B) $0{,}6 < P_c$ (MPa) $< 1{,}3$

Strong dependency on P_c. The results were correlated by

$$r = 0{,}1893\ P_c^{0{,}5584} \qquad (3.2.3)$$

with r in mm/s and P_c in MPa.

(C) $P_c > 1{,}3$ MPa

Hardly any pressure sensitivity until charring occurs, when the regression rate drops instantly and abruptly with increasing pressure.

In region (A) hardly any soot was observed (see section 3.1). Convection, q_c, being the main heat transfer mechanism in this case can be estimated from the product of the regression rate, r = 0,15 mm/s, the effective heat of combustion of the solid phase (including depolimerization heat etc.), $h_{v_{eff}}$ = 1,3 MJ/kg, and the PMMA mass density, $\rho_F \simeq 1180$ kg/m^3. The result, $q_c \simeq 0{,}23$ MW/m^2, will be used in the following.

In region (B) soot production becomes significant, and radiation is the most probable cause for the increase of regression rate. It is not attempted here to explain why soot is being formed at this particular pressure level and not below 0,6 MPa. It might be due to a decrease in mixing rate, caused by the decrease in inlet velocity corresponding to the increase in pressure (and gas mass density) at constant air mass flow rate. But it will be shown in the following that radiative heat transfer

$$(3.2.4) \quad q_r = \varepsilon_w \varepsilon_g \sigma (T_r^4 - T_{wall}^4)$$

cannot be neglected if soot appears.

In region (C) there is so much soot in the flow that it effectively acts as almost a black body radiator (see 3.4.1). With increasing pressure, the regression rate is therefore no further increased. The charring phenomenon is obviously related to the mechanism(s) of soot formation, and will not be discussed here.

If the net heat transfer to the surface

$$(3.2.5) \quad q_w = \rho_p h_{r_{eff}} r$$

is considered to be the sum of two contributions:

$$(3.2.6) \quad q_w = q_r + q_c'$$

the well-known blocking effect has to be accounted for (see Paul et al., ref. 3 and Muzzy et al., ref. 4). According to Muzzy et al. this can be done by

defining q_c as the convective heat transfer if no radiation would be present, and by writing

$$(3.2.7) \quad q_c' = q_c \, e^{-q_r/q_c}$$

In the pressure region (B) spectroscopy yielded T_r values around 1800 K while T_{wall} is estimated at about 800 K. The wavelength averaged absorption coefficient at the inner surface of PMMA, ε_w, is estimated to be 0,5. If the emission coefficient of the gasmixture, ε_g, is equal to 1, this yields an absorbed radiant heat flux of 0,29 MW/m^2.
The q_c-value of 0,23 MW/m^2 is now adopted, implying the assumption of pressure independent convective heat transfer. This is consistent with the above assumption of a constant gas temperature of 1800 K, since m_a was kept constant during experiments. From the equations (3.2.4), (3.2.6) and (3.2.7), the ratio q_w/q_c is now easily shown to attain values between 1 and 1,5 by calculating this ratio for $q_w = q_c$ and for q_w determined from the above values of q_r and q_c. Since q_w is proportional to r, radiation therefore explains the increase in regression rate by a factor 1,4 if pressure is increased from 0,6 MPa up to 1,3 MPa.

Spectroscopic measurements, to be discussed, revealed a dropping mixture temperature and an increasing ε_g with increasing pressure. The fact that these two trents compensate each other justifies to some extend the above simplifications.

3.2.3 The dependency on mass flow rate for PMMA

The interrelation of mass flow rate, combustion pressure and regression rate of PMMA was investigated (see figure 3.2.5).

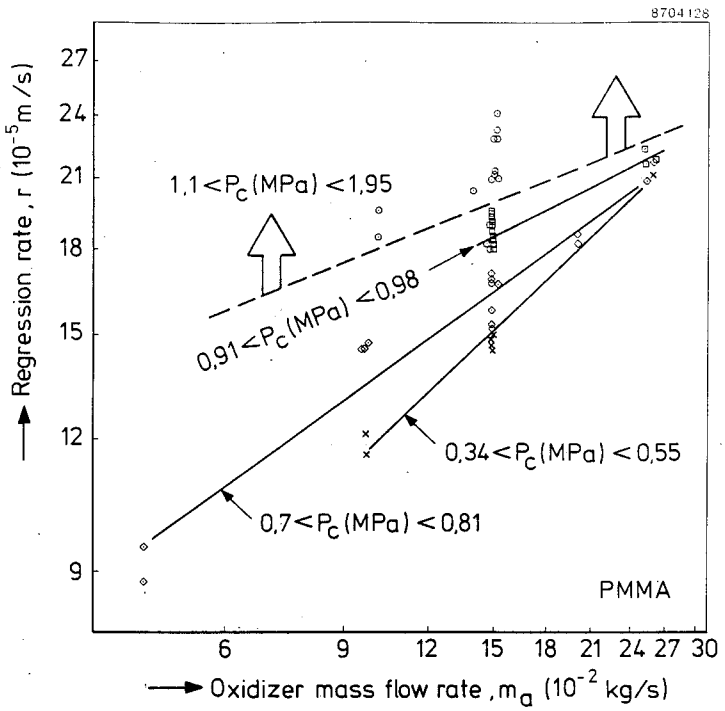

Figure 3.2.5

Effect of mass flow rate on the regression rate of PMMA.

At three pressure levels, the results could be correlated well by correlations of the forms $r = b\, m_a^{\ m}$ and $r = c\, \bar{G}^{\,n}$ (containing essentially the same information, but m_a is a constant during burning and also more accurately known, see also appendix II). Values for the correlation parameters are given in table 3.2.2.

From the correlation exponents and from figure 3.2.5 it is clear that regression is less affected by convection at high pressures than at low pressures. This is in accordance with the conclusion of the previous section (3.2.2) that at high pressures radiative heat transfer constitutes a significant portion of the total heat transfer to the fuel surface.

Table 3.2.2: Correlation parameters for PMMA

$r = a.m_a^b$ $\qquad r = p.\bar{G}^q$

m_a in g/s , $\bar{G}$ in kg/m^{2}s , r in mm/s

P_c(MPa)	$\bar{G}$	m_a	a	b	p	q
0,34-0,55	70-170	100-250	0,0072	0,606	0,0069	0,666
0,70-0,81	35-170	40-250	0,0170	0,452	0,0156	0,508
0,91-0,98	100-170	140-250	0,0381	0,314	0,0363	0,351
PMa	Kg/m^{2}s	g/s	-	-	-	-

3.2.4 Influence of oxygen content and inlet temperature

At a relatively high mass flow rate and a relatively high chamber pressure the effect of oxygen content on the regression rate of PMMA was investigated (see figure 3.2.6). Clearly regression is stimulated by a higher oxidizer concentration.

Spectroscopic measurements, to be discussed in chapter 3.4, showed an increase in flame temperature with increasing oxygen content. This causes an increase in radiative heat transfer according to eq. (3.2.4), but also an increase in convective heat transfer according to the model of Paul et al. (ref. 3). The estimations of section 3.2.2 show that radiative heat transfer is limited, and the levelling off at higher oxygen contents of the regression rate (see figure 3.2.6) suggests that at about 35% oxygen content and P_c = 0,9 MPa radiative heat transfer is maximum. Figure 3.2.4. showed that at 22,5% oxygen context and P_c = 1,2 MPa radiation is maximum, and the fact that these values are not too far off gives confidence in these deductions. If the oxygen content is increased above 35%, the regression rate is further enhanced by an increase in convective heat transfer. The latter can be attributed to the increase in the

temperature of the gas mixture, according to the model of Paul et al. It is noted that Paul et al.have considered fuel mass fluxes that are about one order of magnitude higher than the ones we measured, and hence have been able to neglect radiation in their model.

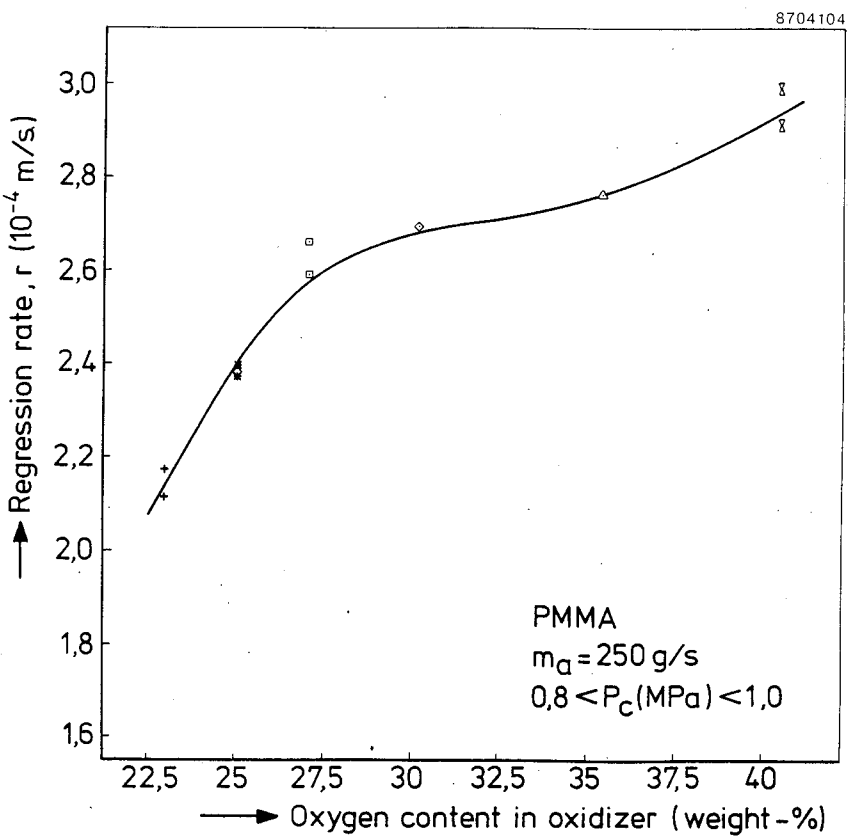

Figure 3.2.6

The effect of oxygen content on the regression rate of PMMA.

Additional and independent support for this assumption of the influence of gas temperature on regression is obtained from PMMA experiments in which the inlet temperature was varied (see figure 3.2.7).

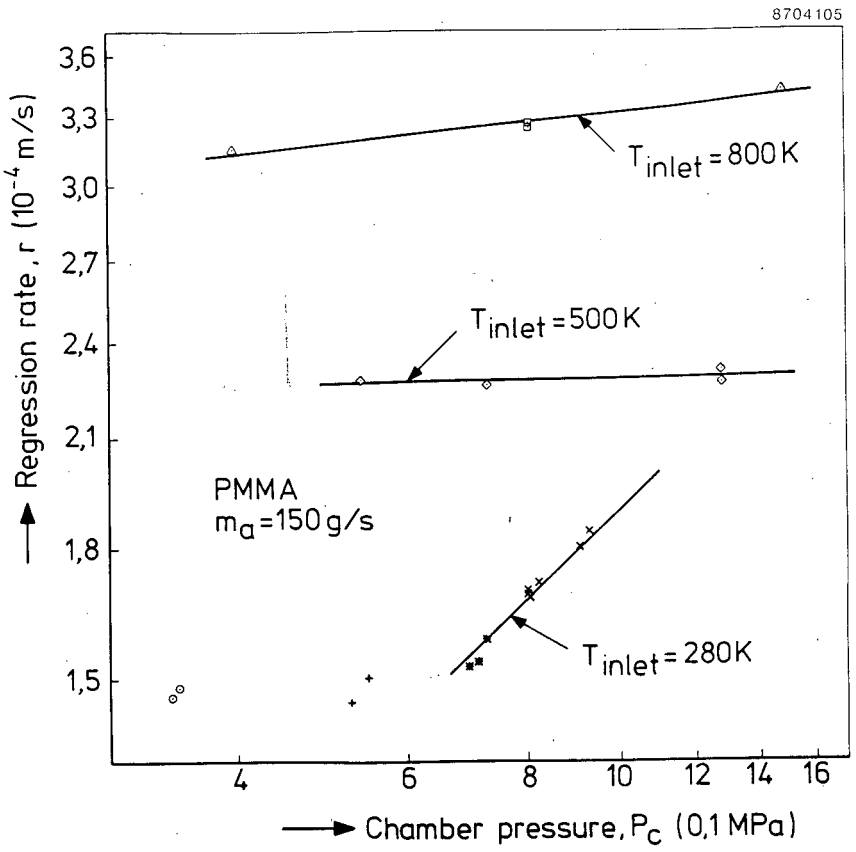

Figure 3.2.7

The effect of inlet temperature on the regression rate of PMMA.

The measurements suggest

- a strong effect of inlet temperature. For pressures lower than 0,6 MPa, r is proportional to $T_{inlet}^{0,79}$.
- almost independance of chamber pressure if P_c is less than 1,5 MPa and T_{inlet} is higher than 450 K.

Since radiation was maximum at about 1,2 MPa, it is clear that the increase in regression rate with increasing T_{inlet} is due to convection. This is confirmed by spectroscopic measurements, to be discussed in the next chapter, that indicate the same flame temperatures and emission coefficients for different values of T_{inlet}.

It is concluded that convection is a prime heat transfer mechanism, which is most clearly manifested at elevated inlet temperatures. Note that the strong dependance on chamber pressure in the range 0,6-1,3 MPa at ambient inlet temperature is still due to radiation. It is also concluded that the temperature in the combustion chamber is a prime regression controlling parameter. The latter has been predicted by the model of Paul et al. (ref. 3).

3.2.5 Dependency on configuration parameters

For h/d_{po} ratios between 0,25 and 0,35, an increase in stepheight increases the regression rate of PMMA (see figure 3.2.8). The measurements were performed at our standard conditions, e.g. m_a = 150 g/s and P_c ~ 0,9 MPa.

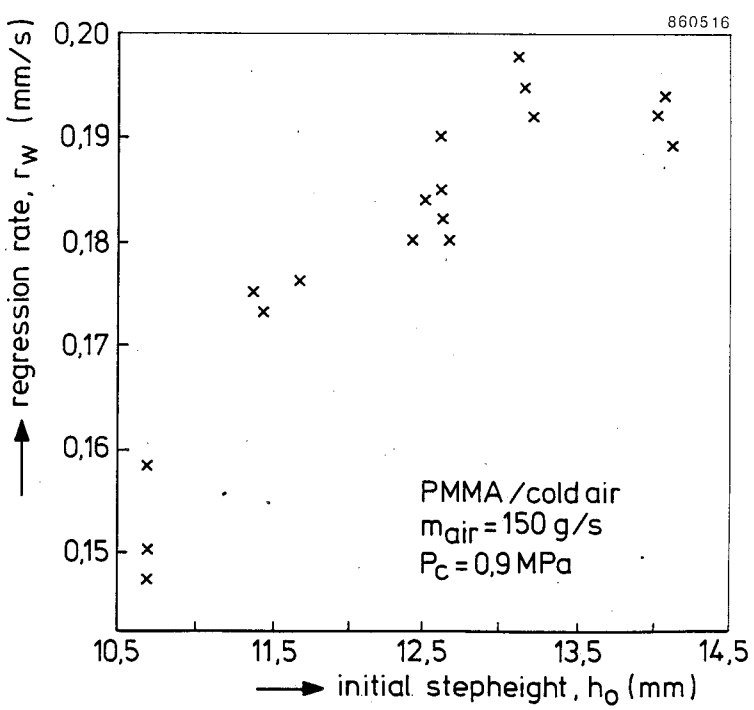

Figure 3.2.8
Effect of stepheight on the regression rate of PMMA.

This increase in regression rate is almost homogeneous downstream of the point of reattachment (see figure 3.2.9).

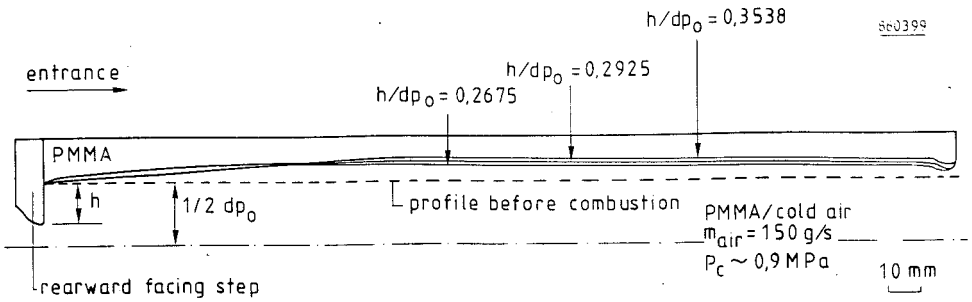

Figure 3.2.9

Grain inner surface profiles after combustion. Influence of stepheight for PMMA.

Figure 3.2.10 shows that the regression rate of PMMA is hardly dependent on grain length.

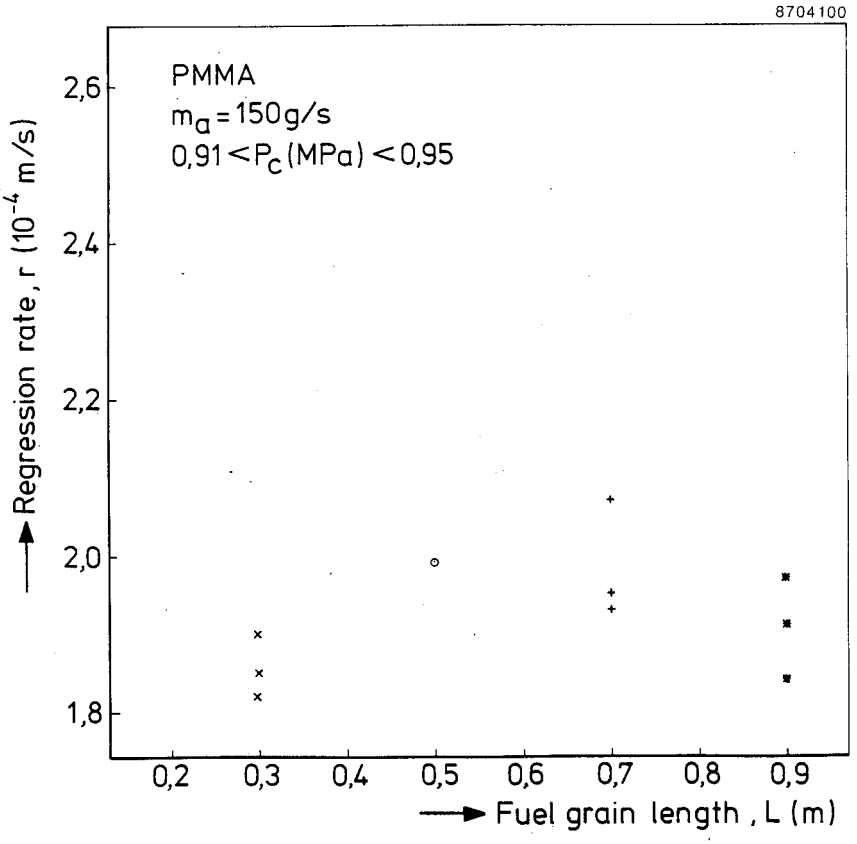

Figure 3.2.10

The effect of grain length on the regression rate of PMMA.

This result is in agreement with the homogeneous burning downstream of the point of reattachment (see figure 3.2.9). A similar observation has been found by Zvuloni et al. (ref. 5).

3.2.6 Instantaneous regression rate

During some testruns, the local instantaneous regression rate was measured with an ultrasonic pulse echo technique (ref. 6). Results for three different locations from the inlet are shown in figure 3.2.11.

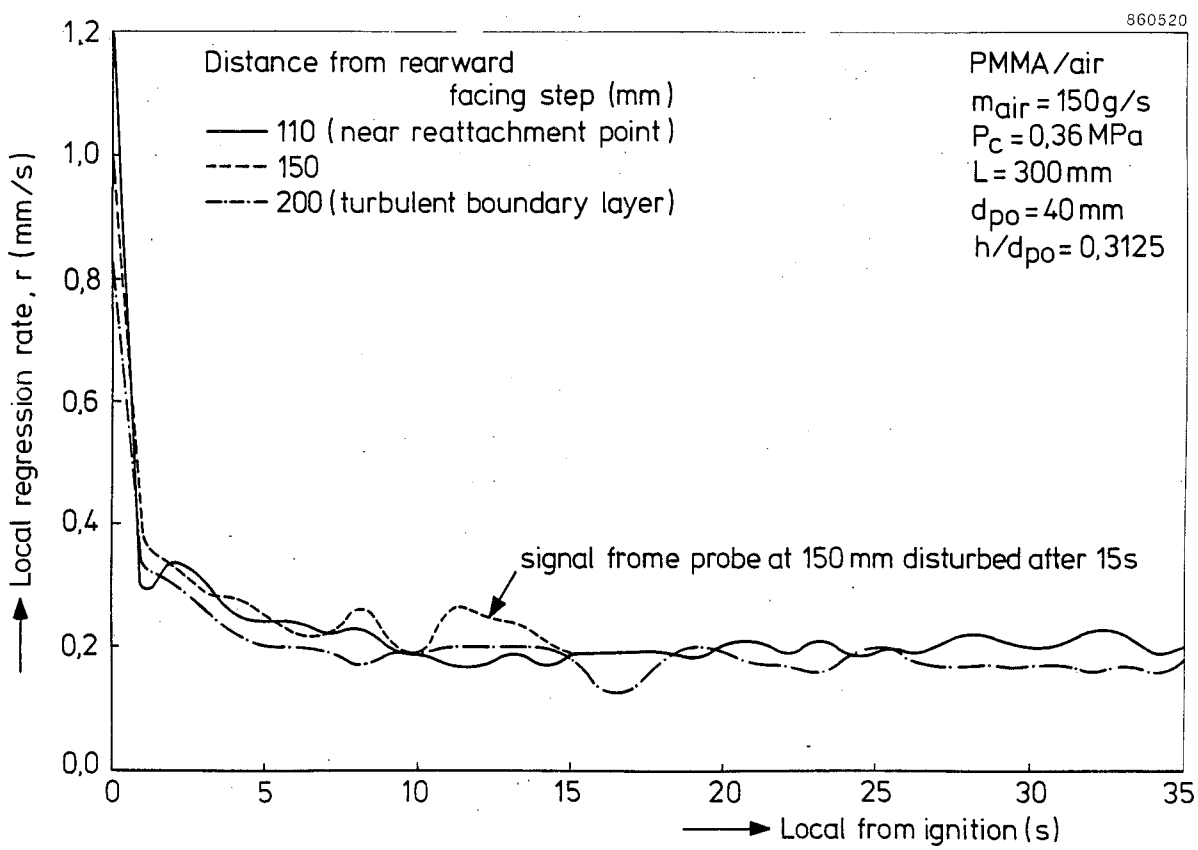

Figure 3.2.11
Specimen of regression rate histories.

Regression is affected by ignition for about 5 seconds (see also section 3.4.3). After that period, regression rate behaviour is seen to be almost

independent of axial location, which is in agreement with the homogeneous burning observed by other means (see section 3.1.2).

3.3 EFFICIENCY

3.3.1 Definitions

The combustion efficiency, η, was defined as the ratio

$$(3.3.1) \quad C^*_{exp}/C^*_{theo}$$

The characteristic velocity depends on fuel properties and was evaluated with

$$(3.3.2) \quad C^*_{exp} = \frac{P_c\ A_t}{(m_a + m_f)}$$

and

$$(3.3.3) \quad C^*_{theo} = \frac{1}{\Gamma} \sqrt{R\ T_c}$$

in which m_a denotes the total air mass flow rate, m_f is calculated from the weight loss, ΔM, during the burning time, t_b:

$$(3.3.4) \quad m_f = \frac{\Delta M}{t_b}$$

A_t is the throat area, Γ denotes the Vandenkerkhove function:

$$(3.3.5) \quad \Gamma = \sqrt{\gamma}\ \left(\frac{2}{\gamma + 1}\right)^{\frac{\gamma + 1}{2(\gamma - 1)}}$$

with $\gamma = C_P/C_V$; $R = R_a/\hat{M}$ with $R_a = 8314{,}32$ J/K.kmol and $\hat{M}$ the molecular weight of the combustion products in kg/kmol. T_c is the equilibrium temperature if burning would be adiabatic and complete. The values of T_c and $\hat{M}$ were calculated with the aid of a NASA computer programme (ref. 7) as a function of pressure and the mixture ratio

$$(3.3.6) \quad \Phi = O/F = m_a/m_f$$

The results for the characteristic velocities and adiabatic flame temperatures of PE and PMMA are gathered in appendix III.

The definition of our standard conditions is given at the beginning of chapter 3.2 as well as in the nomenclature.

3.3.2 Dependency on fuel composition and chamber pressure

Figure 3.3.1 shows the efficiency of PE and PS versus chamber pressure*). No systematic differences between PE and PS results are observed.

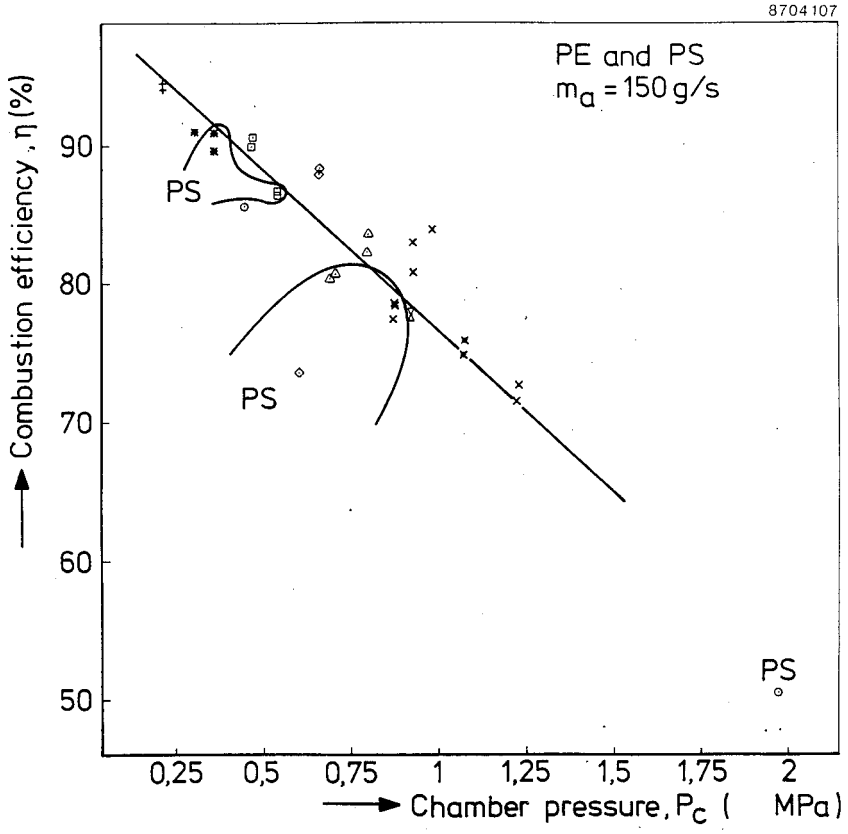

Figure 3.3.1
Effect of chamber pressure on combustion efficiency for PE and PS.

The efficiency is linearly decreasing with increasing chamber pressure. At first glance one is tempted to correlate this trent to the increasing soot production at higher pressures (see sections 3.2.1 and 3.2.2), and the mean lifetime of soot particles in a combustion chamber. However, polystyrene was

*) In this figure and following ones, different symbols for experimental data indicate different experimental conditions (e.g. pressure).

already heavily sooting at 0,3 MPa, and its regression rate showed no distinct dependency on chamber pressure (see section 3.2.1).
In addition, soot production of PMMA depends strongly on chamber pressure below 1,1 MPa (see section 3.2.2), but the efficiency of PMMA in that region is only weakly dependent on pressure (see figure 3.3.2). Note that intrusive probes create additional vortex structures, enlarge turbulent mixing and apparently increase efficiency (figure 3.3.2).

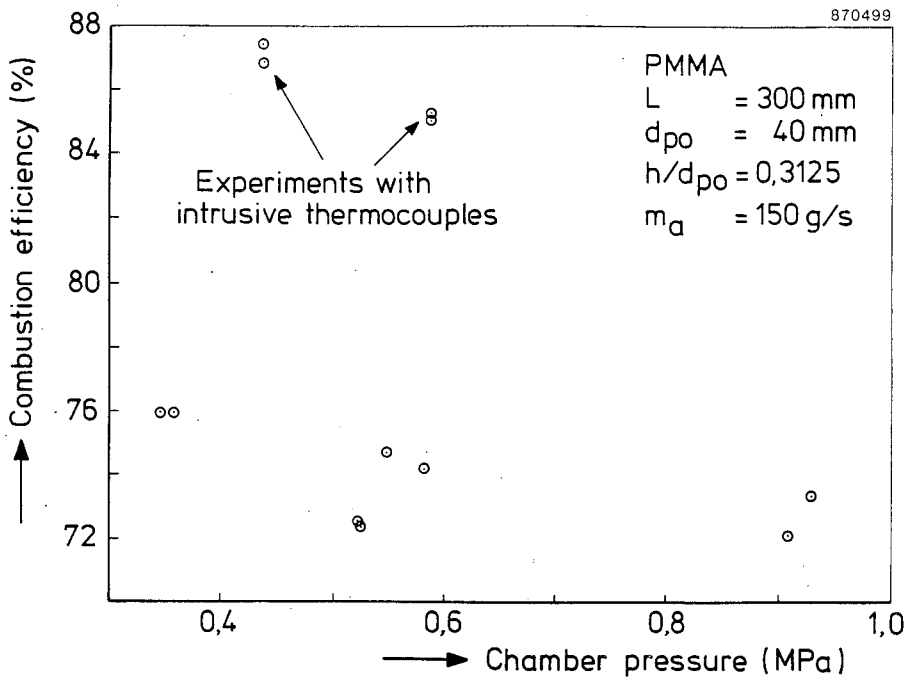

Figure 3.3.2
Effect of chamber pressure on the combustion efficiency of PMMA.

From these observations it is obvious that combustion efficiency is not uniquely determined by the regression rate and is not necessarily connected to soot production. Possible other physical mechanisms and configuration parameters influencing combustion efficiency are mentioned in this and the following sections.
For all three fuels, the value of C^*_{theo} under our test conditions was solely dependent on mixture ratio, and not on pressure. At a constant air mass flow

rate, the theoretical characteristic velocity is therefore uniquely determined by the regression rate. This is confirmed by figure 3.3.3, exhibiting characteristic velocities for PS.

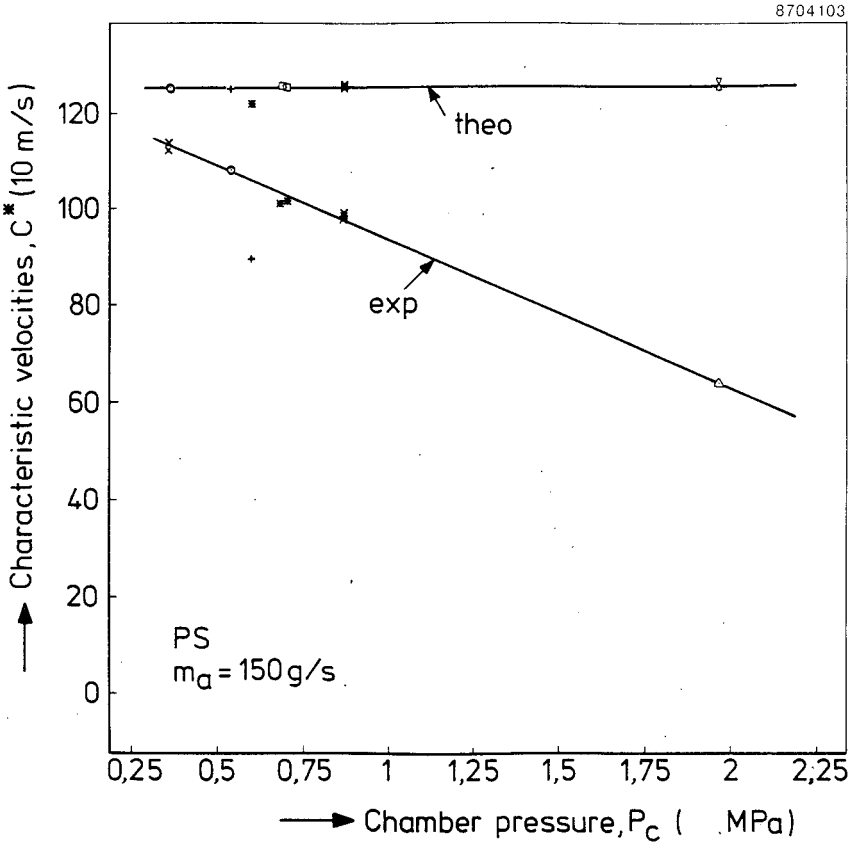

Figure 3.3.3
Effect of pressure on characteristic velocities of PS.

Note that the regression rate of PS is independent of pressure (see section 3.2.1), just like its C^*_{theo}. The scatter in values of C^*_{theo} in figures 3.3.3 and 3.3.4 is due to the scatter in the experimental values of the regression rate at corresponding pressures.
The decrease in C^*_{exp} of PS with increasing pressure can be understood from the decrease in the effective throat area, A_t, caused by the large amount of soot in the exhaust gases. According to eq. (3.3.2), C^*_{exp} is proportional to the

product A_t x P_c. Although P_c is varied by adjusting A_t, the nozzle flow at higher pressures is hampered by the many soot particles.

The combustion efficiency, defined by eq. (3.3.1), can be interpreted as follows. The efficiency is a measure of the deviation of the actual combustion process from thermodynamical equilibrium and complete and adiabatic combustion. In the above case of PS, thermodynamic equilibrium is disturbed by inhomogenous soot distribution due to insufficient turbulent mixing, and in addition burning is incomplete due to the lifetime of soot particles in the combustion chamber. At higher pressures this manifests itself more clearly since the inlet velocity regulating turbulent mixing is inversely proportional to pressure at constant air mass flow rate. This is another interpretation of the decreasing combustion efficiency of PS with increasing pressure.

The combustion efficiency of PE on the other hand is dominated by the dependance of the theoretical characteristic velocity on regression rate (see figure 3.3.4). Note that PE was hardly sooting, as opposed to PS.

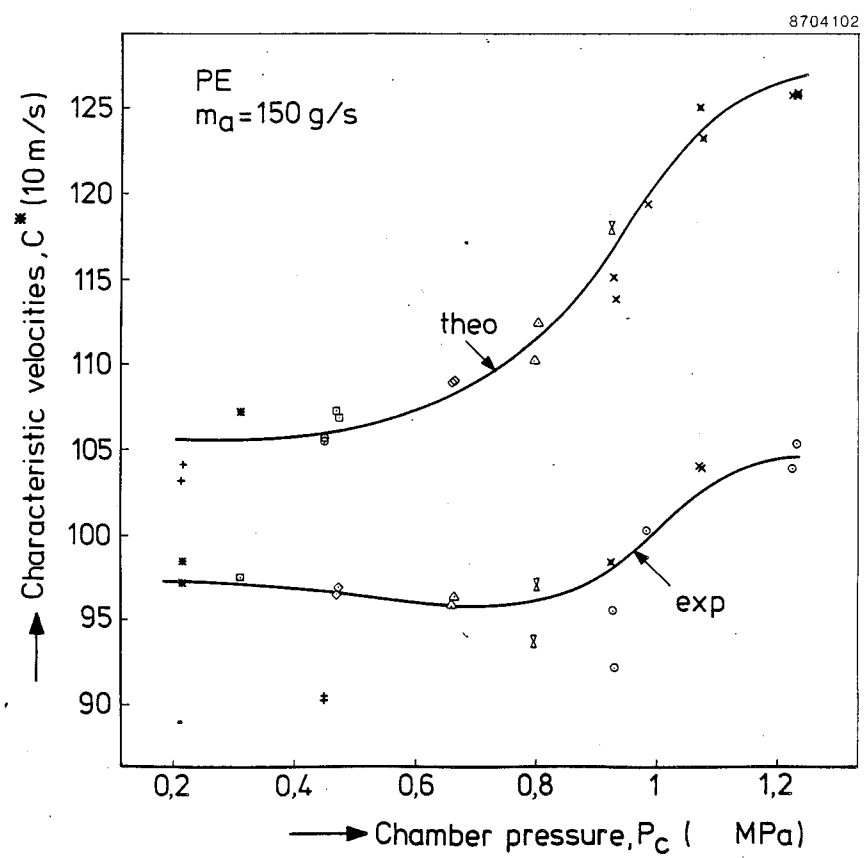

Figure 3.3.4
Effect of pressure on characteristic velocities of PE.

The regression rate and combustion behaviour of PE and PMMA being similar (see the section 3.2), the dependance of C^*_{theo} on pressure for PMMA was expected to exhibit the same trend as for PE (see figure 3.3.5). However, incomplete burning and deviation from equilibrium are not distinctly dependant on combustion pressure for PMMA if pressure is below 1,1 MPa (see also figure 3.3.2).

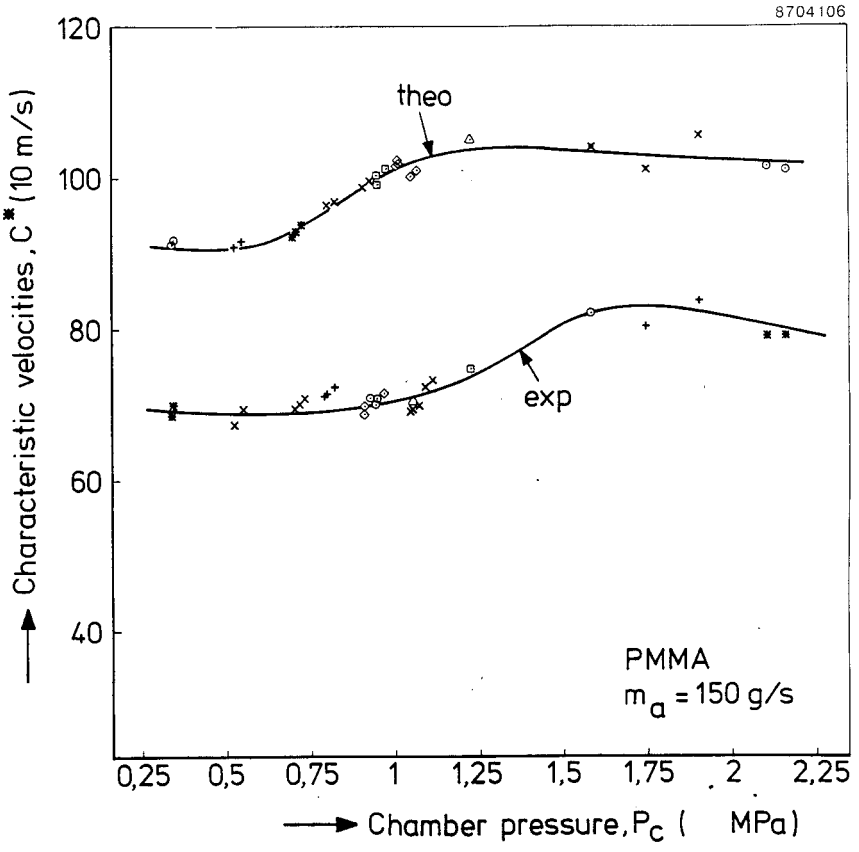

Figure 3.3.5
Effect of pressure on characteristic velocities of PMMA.

Summarizing the results of this section:

- The combustion efficiency, η, for PE, and PS decreases with increasing chamber pressure, P_c;
- Efficiency is conveniently interpreted as a measure of the deviation from equilibrium and complete combustion;

- The dependancy of η on P_c is the same for PE and PS, but different physical mechanisms are responsible for that;
- The behaviour of η for PMMA is similar to that for PE.

3.3.3 Dependency on oxygen content and mass flow rate

For PMMA the effect of the oxygen content in the oxidizer on combustion efficiency was investigated. In view of the relatively large amount of soot at chamber pressure of about 0,9 MPa (see section 3.2.3), this pressure level was selected for this investigation (see figure 3.3.6).

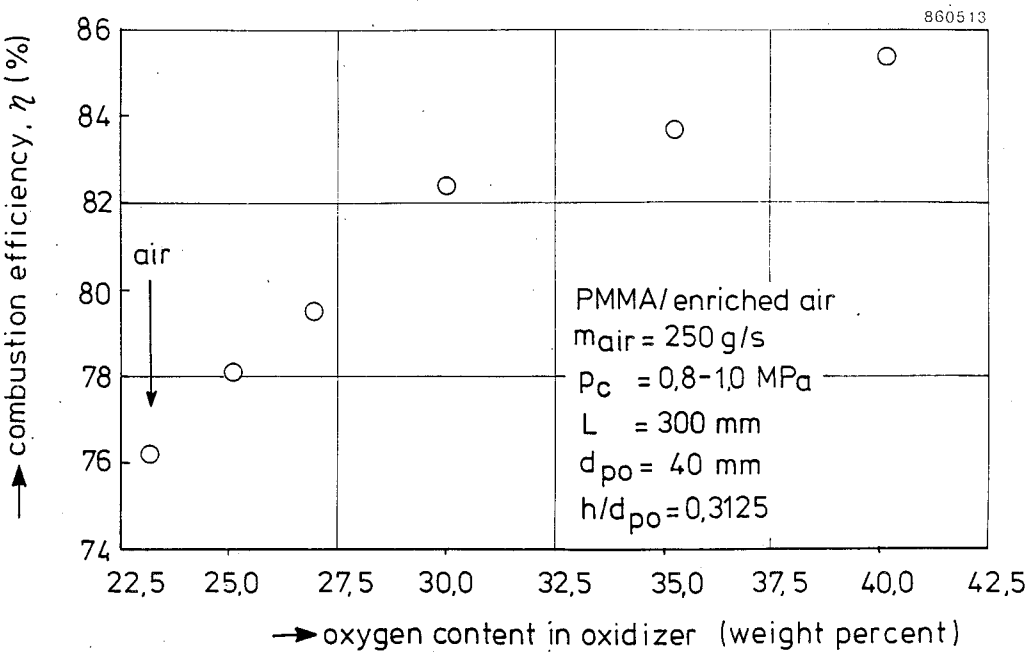

Figure 3.3.6
Effect of oxygen content on the combustion efficiency of PMMA.

The increase of oxygen content clearly increases efficiency. The maldistribution of fuel in the chamber, apparent from the soot, is compensated for by the extra amount of oxydant in the flow, making combustion more complete. This is clearly indicated by the combustion efficiency, as was already discussed in the previous section (3.3.2).

For PMMA the effect of mass flow rate on combustion efficiency was investigated in the range 100-250 g/s. Only a weak dependancy was observed (see figure 3.3.7).

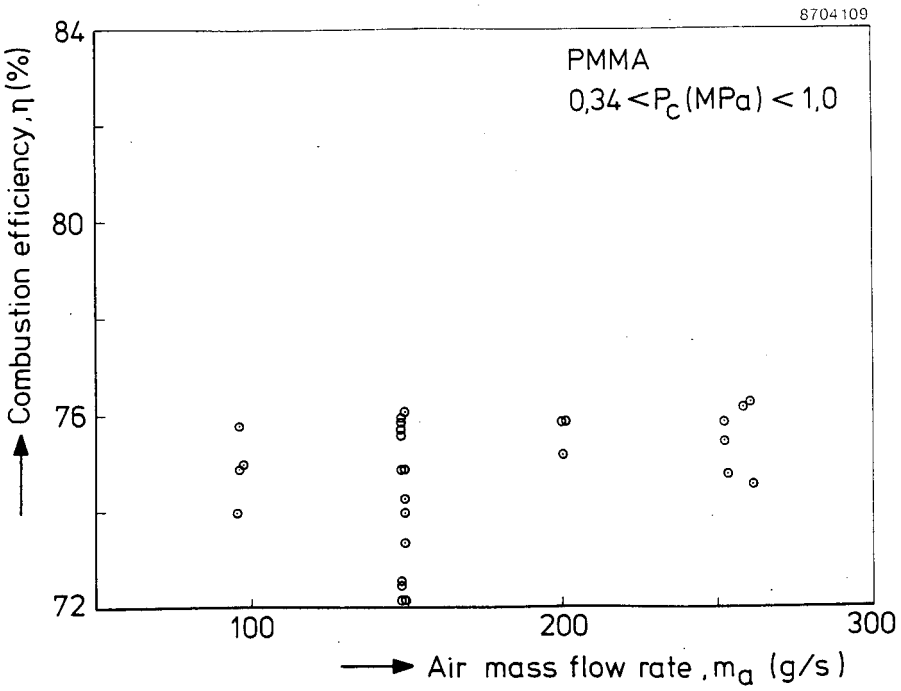

Figure 3.3.7
Effect of the mass flow rate on the combustion efficiency of PMMA.

3.3.4 Dependency on configuration parameters

The effect of the following changes in configuration parameters on the combustion efficiency of PMMA were investigated:

-A- stepheight from 10,5 to 14,5 mm with constant inner bore of the fuel grain (40 mm);
-B- fuel grain length from 0,3 to 0,5 m;
-C- aft mixing chamber length, 0,17 and 0.27 m.

All measurements were performed at a pressure level of about 0,9 MPa since soot production was relatively large at these pressures (see section 3.2.2) and soot was expected to amplify the dependency on configuration parameters.

-A-

Increasing the stepheight, h_o, slightly reduces combustion efficiency (see figure 3.3.7). By increasing h_o, the recirculation zone becomes larger, and hence the flow region with minimum regression rate becomes more important.

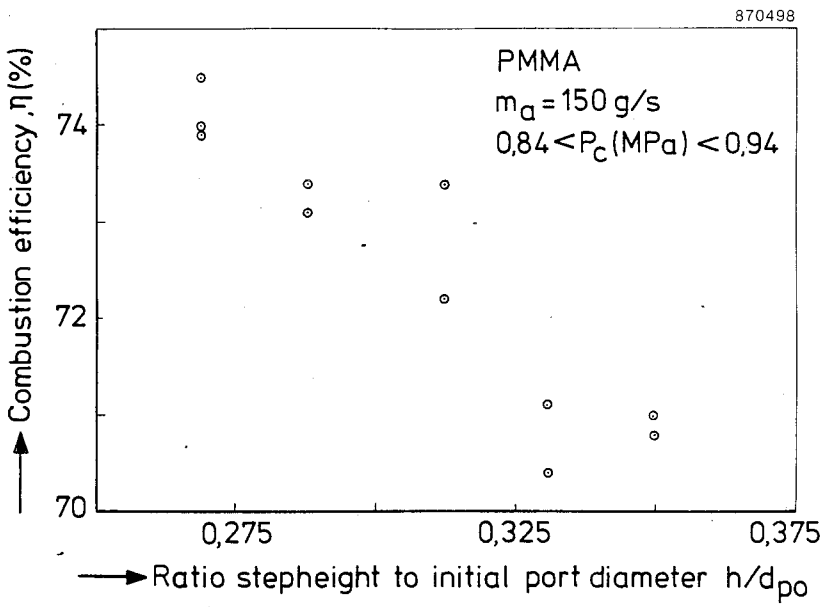

Figure 3.3.8

Effect of stepheight on the combustion efficiency of PMMA.

Inhomogenity becomes more apparent, and again the combustion efficiency indicates this deviation from the one-dimensional flow type.

-B-

The longer the grain length, the longer the average residence time of soot and combustion gases in the chamber, and the more complete the combustion process. This too is indicated by the combustion efficiency (see figure 3.3.9).

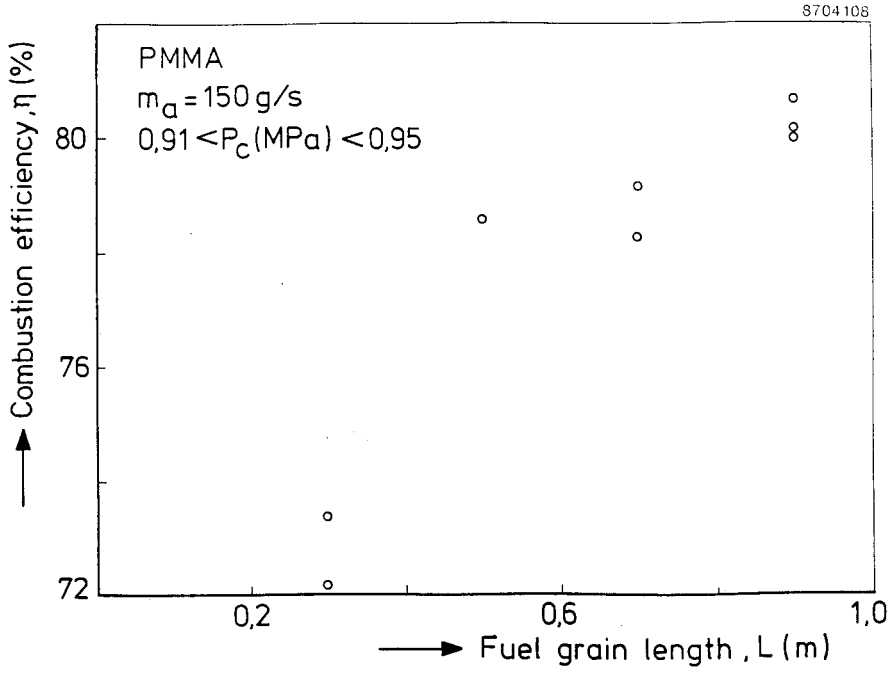

Figure 3.3.9
Effect of fuel grain length on the combustion efficiency of PMMA.

Soot and fuel gases from the downstream end of the fuel grain are never completely burned. If the extent of this part of the fuel grain is negligible with respect to the remaining part, an increase in grain length will hardly affect efficiency. This is reflected in figure 3.3.9 by the tendency to level off at lengths above 0,6 m.

-C-

Obviously the influence of the above mentioned downstream part of the fuel grain can be reduced by increasing the aft mixing chamber length.
During three tests with an elongated aft mixing chamber at about 0,9 MPa, the efficiency was found to amount to about 0,9. This can be compared with the result of figure 3.3.7. The increase of the aft mixing chamber effectuates an increase in efficiency by ca. 20%!
During three tests with an elongated aft mixing chamber at ca. 0,6 MPa, the efficiency was about 0,8. Clearly the presence of soot at the higher pressure region enhances the effect of the aft mixing chamber length.

3.4 TEMPERATURE AND SPECIES

Temperatures in a PMMA combustion chamber were measured with the aid of:
- spectroscopy
- two-colour pyrometry
- thermocouples

PE and PS fuel grains are not transparent, and were therefore not used for these experiments.

3.4.1 Spectroscopically determined temperatures

The spectroscopic equipment measures beam and time averaged radiation from the soot in a wavelength region around 380 nm, where the spectral intensity of the Planck curve is proportional to $\simeq T^{20}$. If it is assumed that no appreciable absorption of radiation from soot occurs along the optical path of detection, e.g. by cooler soot particles, only the maximum temperatures along that path are derived, because of the high exponent in T^{20}.
Attempts to obtain reliable values of temperature from rotational lines of diatomic molecules (CH, OH, C_2) failed, because of the low signal to noise ratio in the observed line intensities.

Spectra of radiation from soot were analysed. It was assumed that the variation in the soot spectral absorption coefficient could be neglected in the wavelength region of 8,5 nm at 380 nm, covered by the multi-channel detector in the spectrograph using 2400 lines/mm grating. With this assumption, the spectrum of the radiating soot can be considered to be one of a grey body with the same temperature. The spectrum of a grey body is known from the Planck formula as a function of wavelength and temperature.

From a calibrated tungsten ribbon lamp, comparison spectra in the above mentioned wavelength region were recorded at temperatures between 1300 K and 3000 K at 100 K intervals.
Although the absorption coefficient of tungsten varies with temperature, it is almost constant in the wavelength region used (variation $< 0,2\%$). Hence, in this wavelength region the spectrum of radiating tungsten can be considered to

be the same in this wavelength region as that of a grey body with the same temperature.

Soot radiation spectra from the combustion chamber have been compared with the above mentioned comparison spectra of known temperatures. The flame temperature, which almost equals the soot temperature, is the temperature assigned to that comparison spectrum which fits best, see figure 3.4.1.

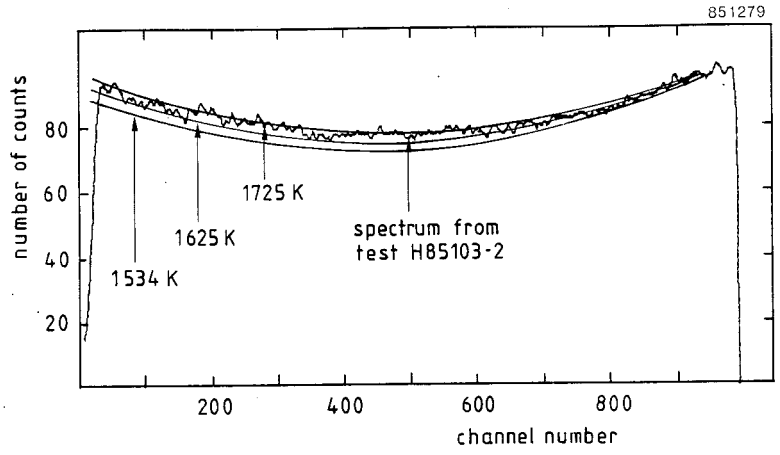

Figure 3.4.1

Principle of temperature determination with the aid of reference spectra obtained from a calibrated tungsten ribbon lamp.

During each test run usually 32 flame spectra were recorded successively at intervals of about 1 s. Data transfer required 33 ms after 1 s exposure time.

In figure 3.4.2 spectra of a flame at a mean pressure of 0,53 MPa, taken at 6, 12, 18, 24 and 30 s after ignition, are shown, while Tables 3.4.1 through to 3.4.3 summarize the results of temperatures, determined from spectroscopy, of typical combustion experiments. The inaccuracy in the temperatures found is 50 K, unless specified otherwise.

Figure 3.4.2 (opposite page)

Time history of spectral emission. Spectra not corrected for background (about 430 counts), nor for non-uniform sensor sensability. Sampling time 1 second per spectrum. PMMA/cold air (149 g/s air mass flow rate). Chamber pressure 0,53 MPa. Axial distance from inlet 225 mm.

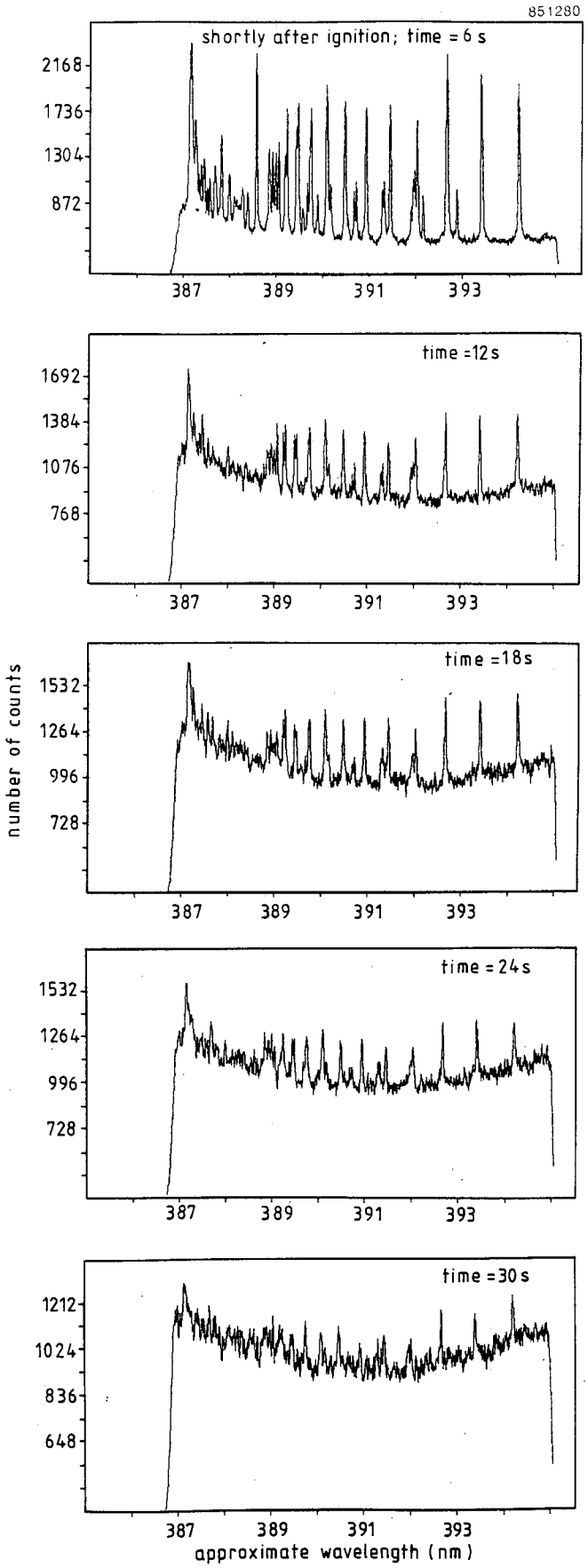
851280
shortly after ignition; time = 6 s
2168
1736
1304
872
387
389
391
393
time =12s
1692
1384
1076
768
387
389
391
393
time =18s
number of counts
1532
1264
996
728
387
389
391
393
time = 24s
1532
1264
996
728
387
389
391
393
time =30s
1212
1024
836
648
387
389
391
393
approximate wavelength (nm)

Table 3.4.1 Results of spectroscopic measurements from PMMA combustion experiments with cold air. Temperature accuracy 50 K, unless specified otherwise.

Testnumber	Distance from entrance (mm)	p_c (MPa)	m_a (g/s)	Temperature (K) time after ignition (s) 6	12	18	24	30	Remarks
H851003-2	75	0,92	262	2300	2300	2050	2050	1950	In recirculation zone
H851112-1	110	0,84	150	2050	1850	1600	1750	1750	
H851107-3	110	0,88	150	1750	1750	1600	-	-	Near re-
H851111-4	110	0,90	150	1850	1850	1750	1750	1750	attachment
H851108-1	110	0,92	150	1600	1600	1500	1600	1600	point
H851018-5	225	0,35	149	a)	a)	2800	2800	2800	b)
H851018-2	225	0,55	150	2550	2300	1050	2050	1950	c)
H851008-1	225	0,78	96	1950	1850	1850	1750	1600	
H851028-2	225	0,80	149	1850	1600	1600	1600	1750	developing
H860218-2	225	0,80	150	1870	1660	1680	1720	1680	d) boundary
H851017-1	225	0,91	201	2050	1950	1850	1750	1750	layer
H851016-2	225	0,93	150	1750	1850	1850	1750	1850	
H851028-4	225	0,95	149	1750	1600	1750	1750	1600	
H851021-2	axial	0,34	150	a)	a)	a)	a)	a)	e)
H851022-1	axial	0,53	149	2800	2400	2200	1950	1950	f)
H851025-1	axial	0,71	149	2050	2050	1750	1600	1750	
H851025-3	axial	0,82	149	1750	1600	1600	1750	-	

a) Temperature between 3000 K and 5000 K
b) 100 K accuracy, decreasing line intensity
c) line intensity decreases to zero at increasing pressure
d) accuracy 30 K
e) irregular decreasing line intensity
f) 100 K accuracy, weak line intensity decreasing to zero at increasing pressure

Table 3.4.1 gives the results of the experiments, carried out with cold air. The locations of the optical path of detection were at 75 mm, 110 mm and 225 mm from the entrance of the fuel grain, while in some cases spectra of axially emitted light were recorded.

Table 3.4.2 Results of spectroscopic measurements from PMMA combustion experimer with air of 800 K, Temperature accuracy 50 K, unless specified othe wise.

Testnumber	Distance from entrance (mm)	p_c (MPa)	m_a (g/s)	Temperature (K) time after ignition (s) 6	12	18	24	30	Remarks
H860225-10	150	0,40	146	-	3600[a]	2400	-	2400	developing
H860225-9	150	0,81	149	2250	2040	2010	1740	1850	b) boundar
H860225-8	150	1,49	149	-	1820	-	1550	-	b) layer

a) accuracy 200 K
1b accuracy 30 K

Table 3.4.2 gives the results of experiments with inlet air heated to 800 K.

Table 3.4.3 lists the results of experiments with cold, oxygen enriched air.

Table 3.4.3 Results of spectroscopic measurements from PMMA combustion experimen with oxygen enriched air. Temperature accuracy 50K, unless specifi otherwise.

Testnumber	Distance from entrance (mm)	p_c (MPa)	m_a (g/s)	oxygen content (weight %)	Temperature (K) time after ignition (s) 6	12	18	24	30	Remarks
H860211-3	225	0,85	254	25	2050	2050[a]	-	-	-	
H860211-4	225	0,85	253	25	2900[a]	2050	2050	-	-	
H860211-5	225	0,90	252	27	2900[a]	2650	2400	2400	2300	develo ping
H860217-1	225	0,96	246	35	-	-	2550	2600	2660	b) bou dary layer
H860217-3	225	0,97	248	40	2910	2780	2780	2780	3110	b)
H860217-2	225	1,00	256	40	2780	2820	3090	2950	2850	b)

a) accuracy 100 K
b) accuracy 30 K

Some temperatures could only be estimated to be in the range 3000 K - 5000 K, according to the radiation spectra. Another indication of such high temperatures is the increased relative intensities of the high numbered rotational lines of CH with respect to the intensities of the same lines in a 2050 K butane flame.

From the above tables two major effects are observed:
- at pressures roughly below 0,6 MPa, the temperatures are significantly higher than those at higher pressures,
- the variation in temperature during an experiment is considerably larger at low pressure than for experiments carried out at higher pressures.

At higher pressures, experiments carried out with cold air (Table 3.4.1) have a tendency to level off at temperatures of 1600 K to 1800 K. Although only a few experiments were carried out with heated air (Table 3.4.2), the results show the same tendency.
Table 3.4.3, where oxygen enriched air was used, shows different results. All experiments took place at pressures above 0,8 MPa and temperatures are significantly higher than those of experiments with not enriched air. The tendency of a decreasing temperature during test runs with cold air is not observed here. On the contrary, some test runs have a tendency of increasing temperature.

From visual observation of the burning fuel grain it is noted that at low pressure hardly any soot is present, while at higher pressures the presence of soot is clearly seen and seems to increase with increasing pressure.
As a result, radiation will increase, leading to an increase of regression rate. This phenomenon has already been discussed above, but it is interesting to verify whether the emissivity of the gas/soot mixture will be pressure dependent as well. In the optical wavelength region chosen, no radiation of the gas itself was measured. This implies that only soot can contribute to the emission coefficient (e.c.) of the flame along the optical path in this wavelength region. For low values of e.c., this e.c. is directly related to the soot concentration. Relative values of e.c. were obtained from the ratio between spectral intensities measured and the calculated spectral intensities of black body radiators at the determined temperatures.

The results are shown in Figure 3.4.3 for air at ambient temperature, air at 800 K and oxygen enriched air.
Comparison of the spectral intensities from the flame and from the calibration lamp showed that the emission coefficient is unity at about 1700 K.

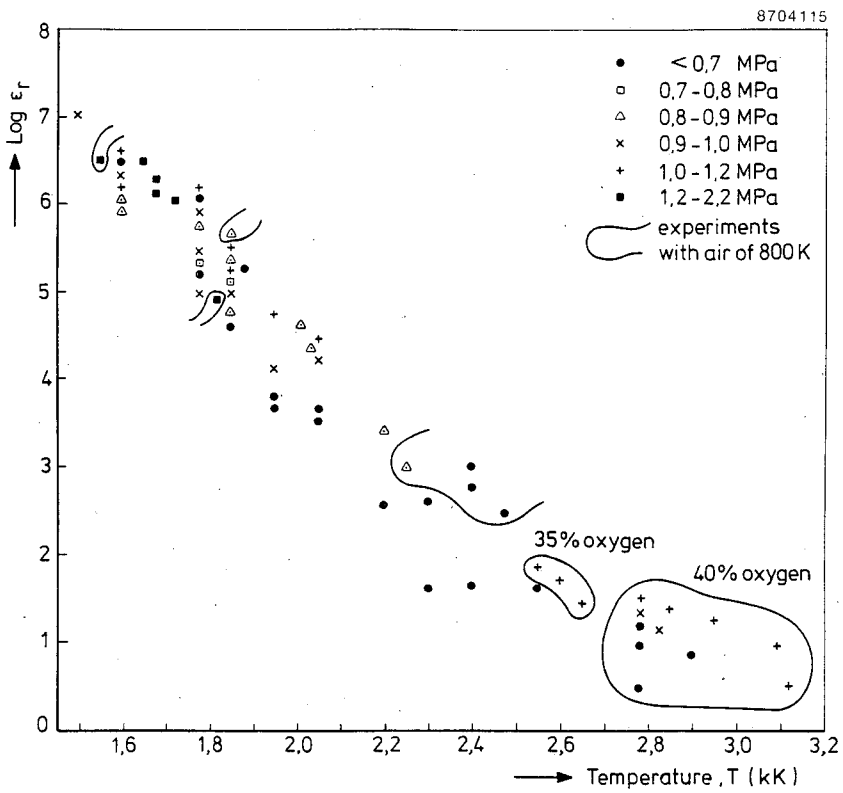

Figure 3.4.3
Relative emission coefficient versus temperature. For clarity some data points were omitted. The absolute emission coefficient is unity at about 1700 K. The error in log ε_r is about 0,5.

For air at ambient temperature and 800 K it is seen that the e.c. decreases with temperature and increases with increasing chamber pressure (despite the lowering temperature). There is no distinct discrepancy between the results of air at ambient temperature and air at 800 K.

For the experiments with oxygen enriched air, the e.c. is remarkably lower. From this it may be concluded that oxygen enrichment favours good combustion

which manifests itself in a lower soot production and a higher combustion temperature (see Table 3.4.3). In addition the observed e.c.-pressure dependancy supports the assumption made earlier that the observed increase in regression rate with increasing pressure is caused by radiation from soot. When the gas/soot mixture becomes optically dense, an increase in soot concentration does not yield an increase in radiation, which may explain the observed leveling off of the regression rate at higher pressures.

3.4.2 Pyrometric temperature results

During a few months of operation, the following results were obtained with the two-colour pyrometer:

1. Temperatures obtained did not vary significantly from those obtained with spectroscopy (see section 3.4.1);
2. Measurements at the reaction zone, at 0,25 * L from the entrance, showed temperature fluctuations which increased from about 300 K at 6 s after ignition to about 600 K at the end of the experiment (ca. 30 s after ignition). Each fluctuation occurred within a few hundreds of a second. The RC-time of the pyrometer was set at 0,01 s, but a setting at 1 ms did not show a significant difference in output of these fluctuations;
3. At 0,25 * L from the entrance, the mean temperature of the reaction zone gradually decreases with about 300 K during an experiment, as also observed with spectroscopy (see section 3.4.1);
4. At 0,75 * L from the entrance, the temperature fluctuations are about 200 K, while the mean temperature decreases with about 150 K during an experiment.

The large temperature fluctuations are attributed to the oscillatory shedding of the large vortex structures of the recirculation zone (see section 3.1.1). Note that the two-colour pyrometer measures temperatures while the radiation detector, whose results were already discussed in the context of the vortex shedding in section 3.1.1, measures radiation intensities. The temperature fluctuation is probably due to the difference in the mean temperatures of the recirculation zone and the remaining part of the combustion chamber. Each time

a vortex sweeps through the grain and diffuses in the downstream end of the grain, the temperature is lowered at these places.

Since only mean values of the temperature along the optical path of detection are determined, the pyrometer will be attached to a mechanism in order to scan the area of detection along the radius of the flame. With help of a shell model of the flame and a proper conversion technique, it is intended to determine the flame temperature as a function of the distance to the axis.

3.4.3 Chemical compounds in the combustion chamber

With the 600 l/mm grating, yielding a wavelength region of about 35 nm on the detector, spectra were recorded between 300 nm and 600 nm by adjusting the central wavelength of the spectrograph in order to find specific spectra of chemical compounds.
To minimize the disturbing influence of soot as much as possible, the location of the optical path of detection inside the combustion chamber was chosen at a distance of 225 mm downstream of the inlet.
At a mass flow rate of about 150 g/s and at pressures of about 0,5 MPa, spectra of CH, C_2 and OH were found, see figure 3.4.4. Except for soot, no other spectra could be found.
The spectrum of OH was recorded at 309 nm via ultraviolet optics between the slit of the spectrograph and the combustion chamber through a quartz window, with the optical detection path in axial direction. The efficiency of this optical train was also about 30%.

After ignition, the intensity of the OH-spectrum dropped by a factor of approximately 30 during the first 5 seconds, after which it remained constant. This is attributed to the disappearance of the H_2/O_2 ignition flame.

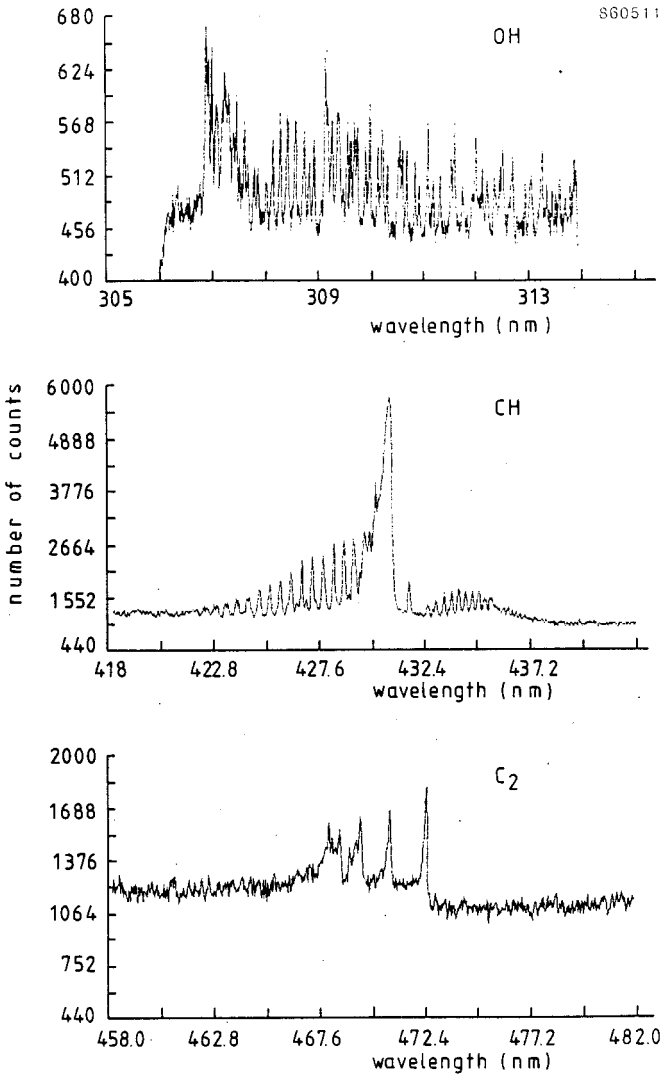

Figure 3.4.4

Spectra of chemical compounds observed during combustion.
PMMA/ambient air; P_c ~ 0,5 MPa.

3.4.4 Thermocouple measurements

Temperature measurements in the two distinct reacting flow zones, the recirculation zone and the developing turbulent boundary layer, were made at different distances from the wall to characterize the flow field temperature.
Pt 10% Rh - Pt thermocouples were used with a diameter of 100 µm, supported by ceramic tubes of 3 mm outer diameter.

The thermocouple probe interfered with the flow, particularly in the near wall region where the reaction was intensified by the action of a horse shoe vortex. The time constant of the thermocouple was found to be about 15 ms.

Table 3.4.4 Thermocouple positions and measured temperatures in inner bore of PMMA fuel grain.
Testconditions: m_a = 150 g/s, p_c = 0,45 MPa, L = 300 mm, d_{po} = 40 mm, h/d_{po} = 0,3125.

Testnumber	Figure	Thermocouple	Distance from entrance (mm)	Distance from wall before test (mm)	Mean temp. (K)
H860130-12	3.4.5	1 2	150 150	20 2	900 1900
H860318-2	3.4.6	1 2	40 40	2 8	1350 1400
H860318-6	3.4.7	1 2	200 265	0 3	1700 1400

Table 3.4.4 lists the thermocouple locations.
The temperature histories, as measured by the two thermocouples at a distance of 150 mm downstream from the entrance (one on the center line, the other near the wall) are shown in figure 3.4.5.
The initial peak represents the hydrogen ignition flame temperature. After about 15 s, the center line temperature remains constant at about 1000 K, while the near wall temperature steadily increases from about 1700 K to 1900 K with peak to peak oscillations of 200 K.

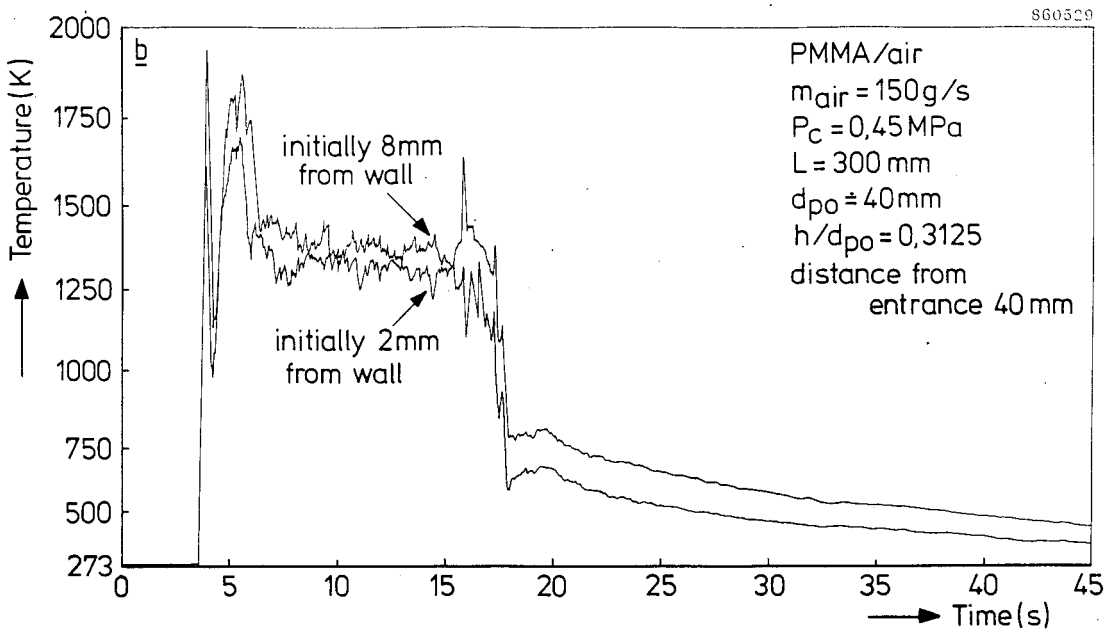

Figure 3.4.5
Specimen of thermocouple readings close to inlet.

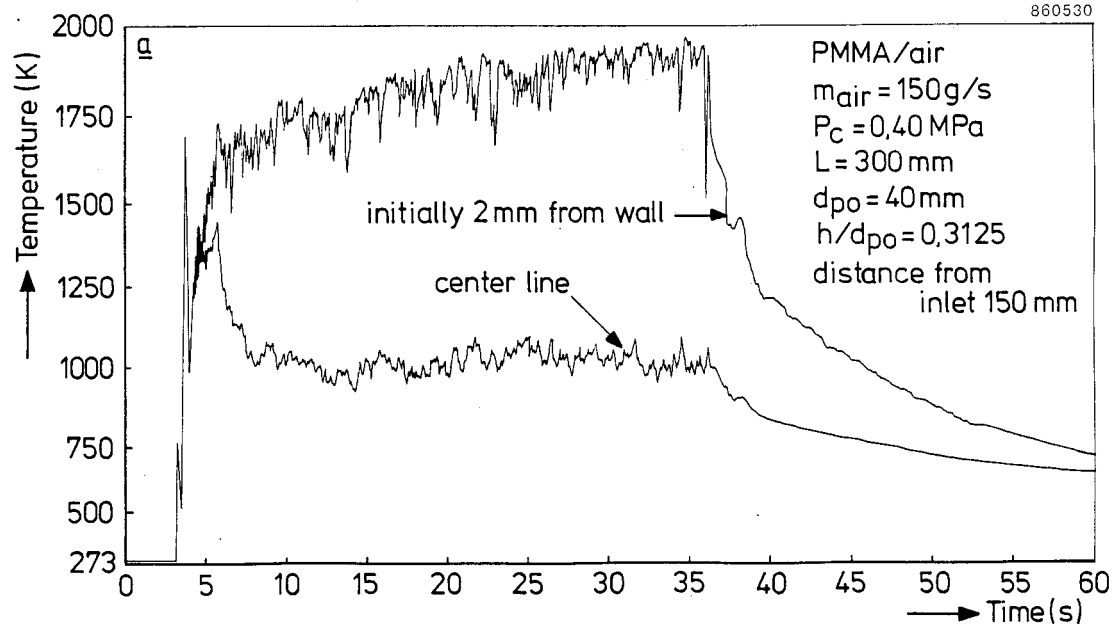

Figure 3.4.6
Specimen of thermocouple readings halfway the grain.

Figure 3.4.6 shows the temperature traces from thermocouples in the recirculation zone at a distance of 40 mm downstream from the entrance. Temperatures of 1350 K - 1400 K prevail in this zone with fluctuations of less than 100 K.

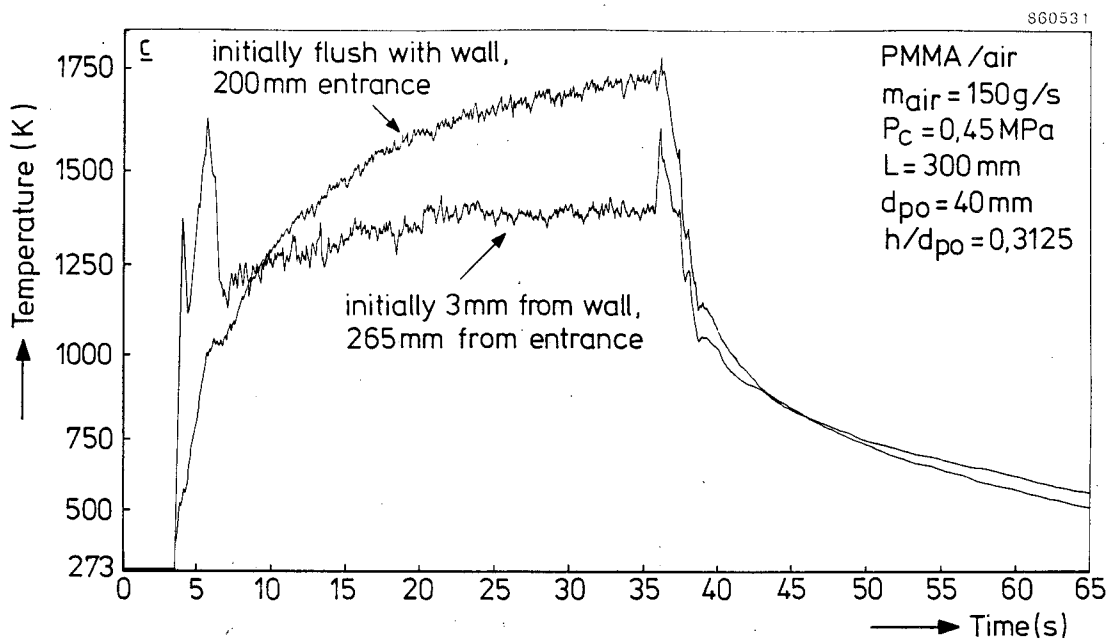

Figure 3.4.7

Specimen of a thermocouple reading near downstream end of the fuel grain.

At 200 mm and 265 mm downstream from the inlet, one thermocouple initially flush with the wall and one at 3 mm from the wall respectively, gave average temperature readings rising from 1000 K to 1700 K and from 1200 K to 1300 K, respectively (see figure 3.4.7).

The thermocouple flush with the wall shows a rapid rise in temperature that may be interpreted as the effect of the wall regression, which effectively pushes the thermocouple junction into the flow and into the reaction zone. As one would expect a decrease in the thermocouple temperature after some time in the case of a thin flame sheet, these measurements seem to indicate that combustion is distributed over a relatively thick layer.

Comparing the results of thermocouple measurements with the results of Tables 3.4.1 through to 3.4.3, it should be noted that

a) the thermocouple experiments took place at pressures between 0,40 MPa-0,45 MPa and at distances between 40 mm and 260 mm from the inlet and

b) in this pressure region only maximum temperatures along the beam are observed with spectroscopy.

Towards the end of tests (see figures 3.4.5 and 3.4.7) the near wall thermocouple measurements tend to 1900 K at a pressure of 0,4 MPa and to 1750 K at a pressure of 0,45 MPa respectively. The corresponding (location and time averaged) spectroscopically determined temperatures lie between 2800 K (at 0,35 MPa) and 1900 K (at 0,55 MPa).

Because of radiation loss and conduction losses of thermocouples, somewhat lower thermocouple measurements (about 100 K - 200 K lower) were bound to take place. Thermocouple measurements take place locally. Since in addition the number of thermocouple experiments was limited, the results are in reasonable agreement with spectroscopic results, the latter always yielding the highest temperatures. Only the measurements that took place in the recirculation zone (see figure 3.4.6) indicate a much lower temperature there. This is in perfect agreement with the interpretation of the temperature fluctuations, observed by two-colour pyrometry, that was given in section 3.4.2. The presence of a low temperature region is furthermore confirmed by the observation, that intensities of spectra, obtained from axially emitted radiation were much weaker than corresponding intensities obtained from radially emitted radiation. Since the derived temperatures remained high, about 1900-2200 K, the decrease in intensity has to be attributed to absorption by cold soot in the recirculation zone.

4 CONCLUSIONS

The combustion behaviour of PMMA, PE and PS in a solid fuel ramjet was studied.

The inner surface of hollow cylinders were burnt with air. The regression rate of PMMA is about equal to that of PE, but about 40% smaller than that of PS. Due to differences in the heat of combustion, the heat release of PE combustion gases is about 60% higher than that of PMMA gases. PS gases release about 100% more heat than PMMA.

The regression rate increases with mass flux due to increasing convective heat transfer. Experiments were performed at mass flow rates below 300 g/s, whence radiative heat transfer could not be neglected. The dependence of regression rate on pressure is absent for PS, and for PMMA and PE it is absent below ca. 0,5 MPa and above ca. 1,1 MPa. The pressure dependent region was attributed to the formation of soot and the increasing importance of radiative heat transfer in this pressure region. Soot production was suppressed by increasing the oxygen content in the supply gases. The increasing of the inlet temperature had no effect on soot production, although it increased regression rate. The temperature in the combustion chamber and convective heat transfer were found to be prime regression controlling parameters.

The combustion efficiency is a convenient measure of the deviation from equilibrium burning and complete combustion. The efficiencies of PE and PS decrease similarly with increasing chamber pressure, although different physical mechanisms are responsible for that Up to a certain grain length, efficiency increases with increasing grain length.

Temperatures were measured with the aid of spectroscopy, two-colour pyrometry and thermocouples. Similar results were obtained. The highest temperatures occur at low pressures and hence at low soot concentrations. Temperature fluctuations of 200 K in the downstream end of the chamber and of 600 K in the upstream end were observed. These fluctuations were connected to the oscillatory shedding of the large coherent vortex structures that are formed in the

recirculation zone directly downstream of the sudden expansion. The shedding rate of these structures was only affected by geometry changes.

REFERENCES

1 Wijchers, T.
A method for spectroscopic temperature measurements in a solid fuel combustion chamber
Memorandum M-53-/Report PML 1985-C7, Delft University of Technology/Prins Maurits Laboratory TNO, 1985

2 Geld, C.W.M. van der
On the direct simulation of vortex shedding
Report LR-513, SFCC-publication nr. 40, PML 1987-C17, Delft University of Technology, 1987

3 Paul, P.J, H.S. Mukunda, V.K. Jain
Regression rates in boundary layer combustion
Nineteenth Symposium on Combustion, The Combustion Institute, pp. 717-729, 1982

4 Muzzy, R.J.
Applied hybrid combustion theory
AIAA paper no. 72-1143; AIAA/SAE 8th Joint Propulsion Specialist Conference, 1972

5 Zvuloni, R., Y. Levy and A. Gany
Experimental investigation of a solid fuel ramjet combustor
Proc. 28 Israel Annual Conference on Aeroautics and Astronautics, 1986

6 Korting, P.A.O.G., H.F.R. Schöyer, C.W.M. van der Geld
On the use of an ultrasonic pulse-echo technique for regression rate analysis. PART II: some experimental results
Report LR-453-II, SFCC-publication nr. 24, PML 1985-C6, Delft University of Technology, 1987.

7 Gordon, S. and B.J. McBride
Computer program for calculation of complex chemical equilibrium compositions, rocket performance, incident and reflected shocks, and Chapman-Jouguet detonations
NASA SP-273, NASA Washington, 1971.

8 Vos, J.B.
The calculation of turbulent reacting flows with a combustion model based on finite chemical kinetics
Ph.D. Thesis, Delft University of Technology, April 1987.

ACKNOWLEDGEMENT

The project "Investigation of a Solid Fuel Combustion Chamber" is financed by the Technology Foundation (Stichting voor de Technische Wetenschappen) and the Management Office for Energy Research (Stichting Projectbeheerbureau Energie Onderzoek). In addition, money and manpower are made available by a special funding of Delft University of Technology (Beleidsruimte), while also manpower, funding and computerfacilities are provided by the Faculty of Aerospace Engineering of Delft University of Technology, and the Prins Maurits Laboratory of the Organisation for Applied Scientific Research (TNO)

APPENDIX 1

Fuel properties

Physical property at 20° C	PMMA	PE	PS	SI unit
molecular weight	100	28	104	kg/kmol
heat of formation	-430,5	-53,8	+18,4	kJ/mol
heat of combustion of gas phase	26,2	46,5	41,5	MJ/kg
mass density	1180	940	1050	kg/m^3
melting point	430-470	370-415	500-520	K
thermal conductivity	0,16	0,40	0,17	W/m K
heat capacity	1,47	2,1	1,8	kJ/kg K
thermal diffusivity	9.10^{-8}	20.10^{-8}	9.10^{-8}	m^2/s

chemical property	PMMA	PE	PS
molecular formula	$(C_5H_8O_2)_n$	$(C_2H_4)_n$	$(C_8H_8)_n$
pyrolysate at ca. 700 K	99% monomer	triplets of alkanes alkenes dialkenes C_nH_{2n+i}	50% monomer 40% "wax" 4% C_6H_6 4% C_7H_8 2% C_9H_{10}
pyrolysate at ca. 1300 K	20% monomer C_2H_4 C_2H_2 CH_4	triplets of alkanes alkenes dialkenes C_nH_{2n+i} (i=-2,0,2)	40% monomer 30% "wax" 10% C_6H_6 5% C_2H_2 5% C_2H_4 5% C_9H_{20} 3% C_3H_4 1% C_7H_8

APPENDIX 2

On correlation parameters

Argumentation for correlating regression rate with mass flow rate rather than mass flux:

- If the mass flux is averaged from its initial and final values and the result, $\bar{G}$, is used for correlating data, the constants in a correlation of the form

  $$r = a\, P^s\, \bar{G}^{\,m}$$

  are usually different from those in a correlation of the form

  $$r = b\, P^s\, m_a^n$$

  m_a being the mass flow rate. However, if the initial and final cross-sectional areas are known, the parameters a and m are easily transfered to b and n and vise versa. In this report only grains with identical initial cross-sectional areas are considered, and hence the correlation procedures contain essentially the same information.

- The mass flow rate is kept constant during a test run. This is done rather accurately with the aid of the SFCC's. However, the cross-sectional area, and hence the mass flux, varies substantially during burning because of the regressing fuel surface. Since fuel burns inhomogeneously the above averaging procedure for $\bar{G}$ is rather crude. Moreover, the regression rate being measured not instantaneously but by weight loss it is far better not to average the mass flux at all since a good average requires knowledge of the instantaneous cross-sectional area and also the instantaneous regression rate. The mass flow rate on the contrary does not change at all.
  Note that for similar reasons only those mean regression rate data that are independent from the total burning time are appropriate for correlating.

APPENDIX 3

Adiabatic flame temperatures and C^*-values for PMMA and PE

The following figures summarize computational results of the NASA computer program of reference 7.

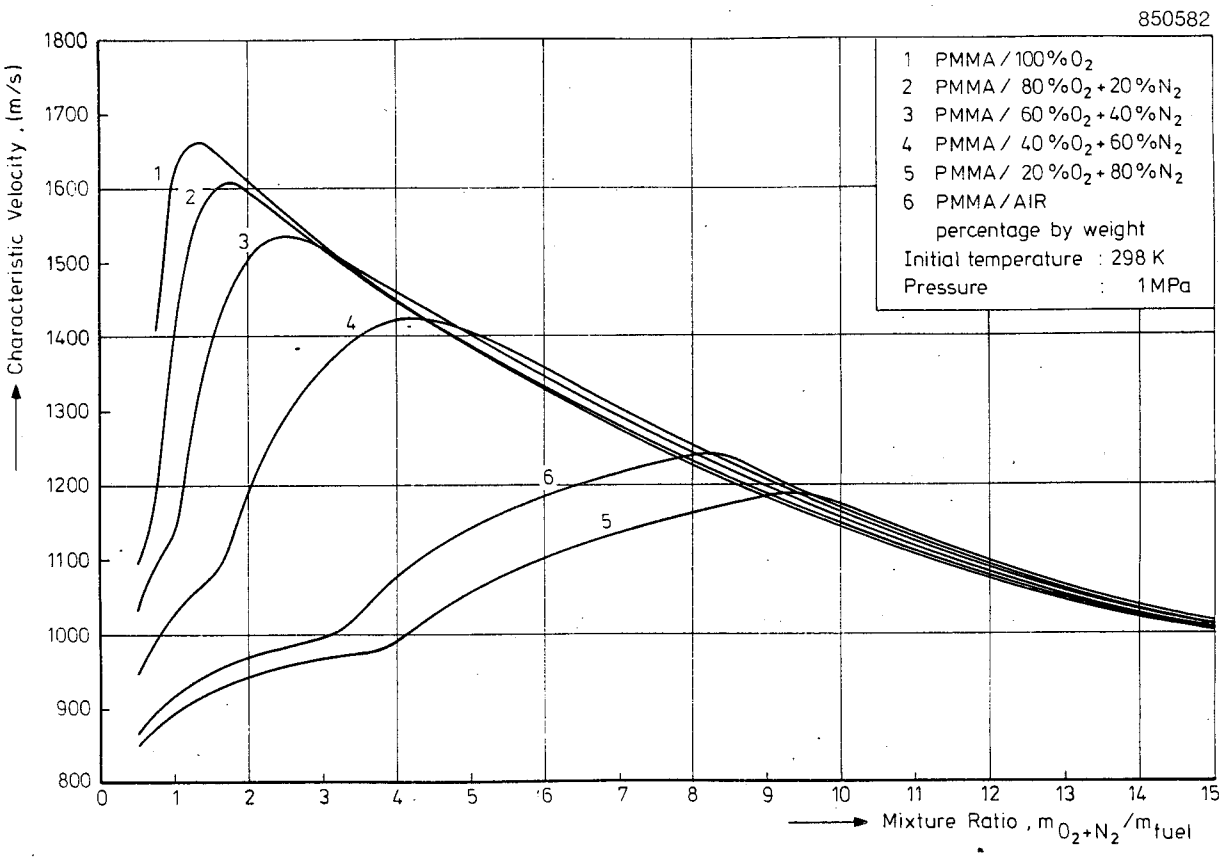

Figure A3.1

Theoretical characteristic velocities of PMMA

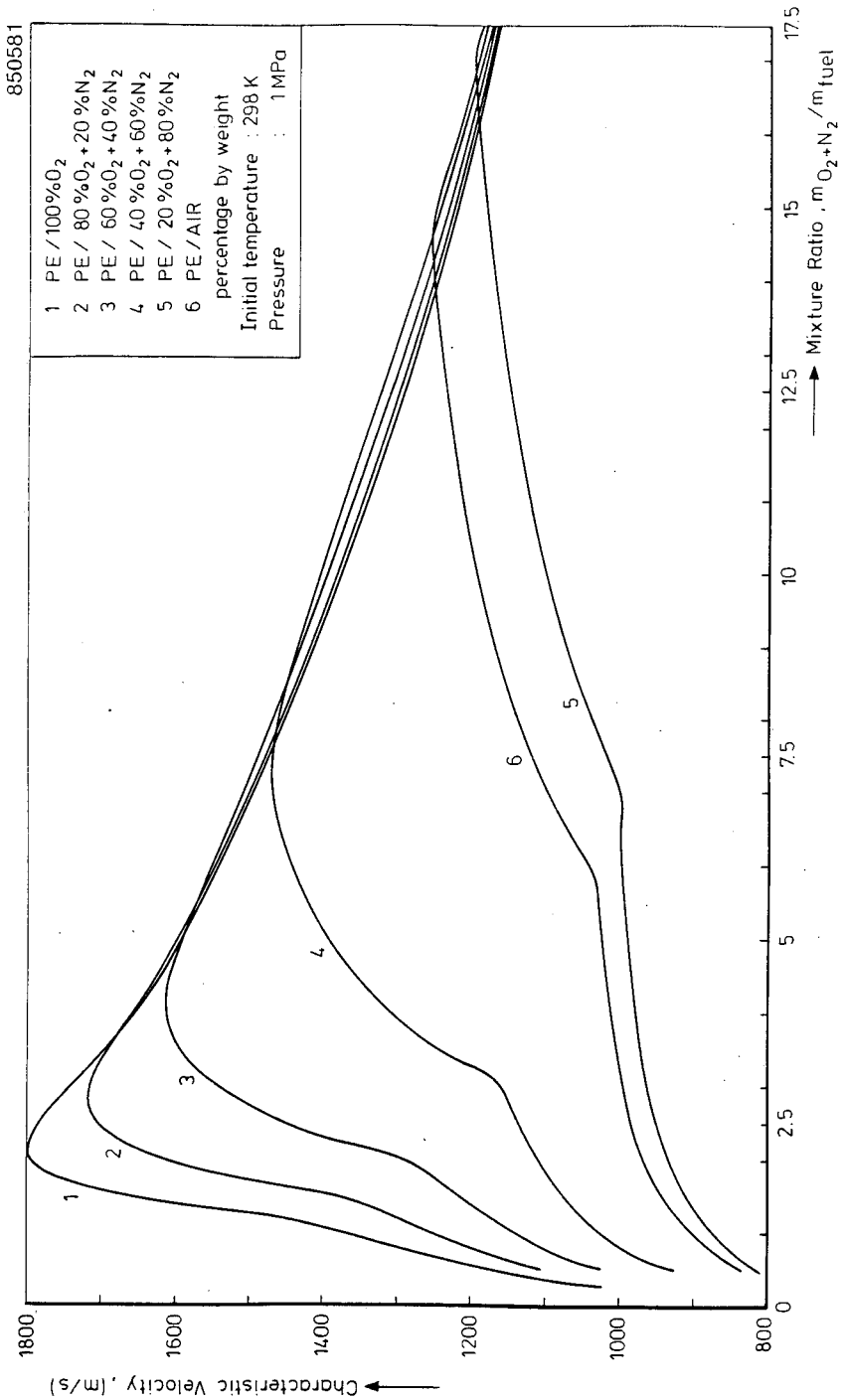

Figure A3.2

Theoretical characteristic velocities of PE

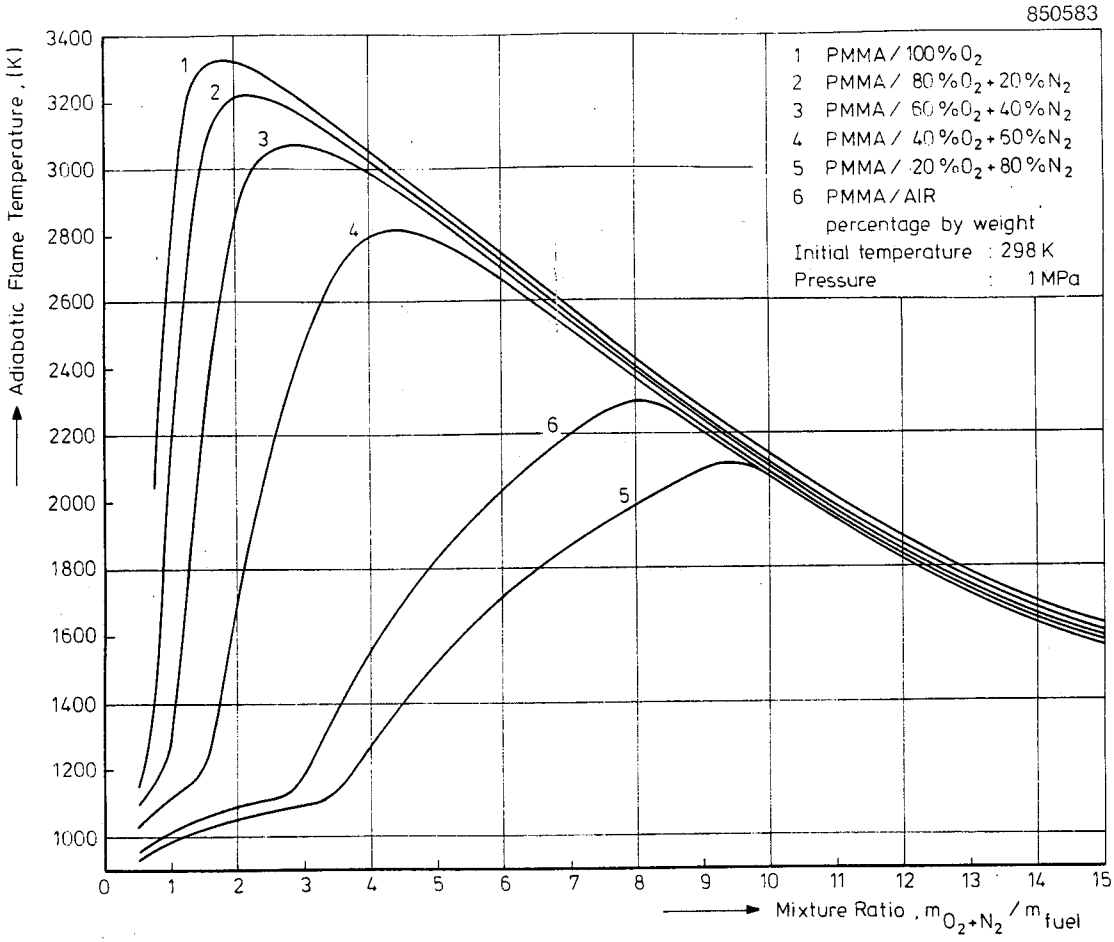

Figure A3.3

Adiabatic flame temperatures of PMMA

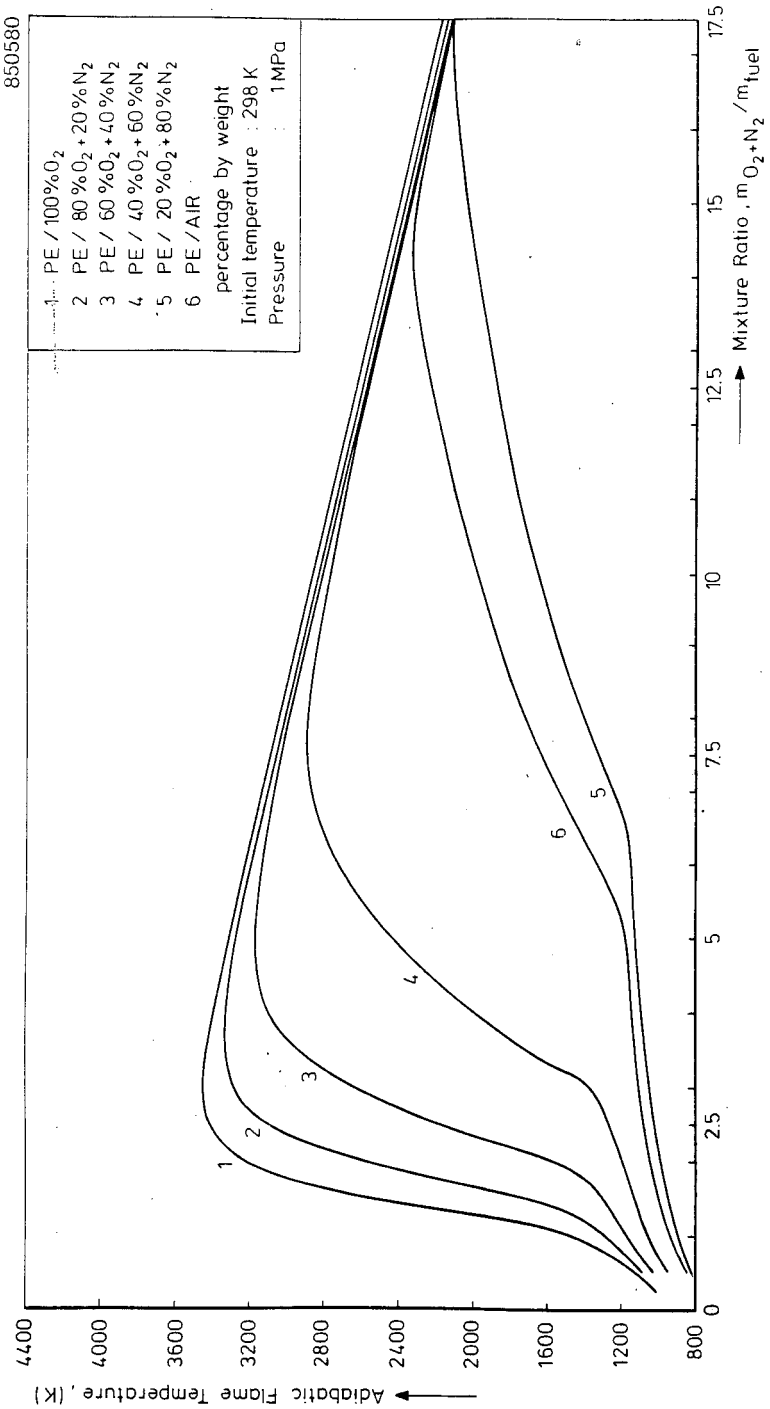

Figure A3.4

Adiabatic flame temperature of PE